MWCNTs of different physicochemical properties cause similar inflammatory responses, but differences in transcriptional and histological markers of fibrosis in mouse lungs

Poulsen, Sarah S.; Saber, Anne T.; Williams, Andrew; Andersen, Ole; Købler, Carsten; Atluri, Rambabu; Pozzebon, Maria E.; Mucelli, Stefano P.; Simion, Monica; Rickerby, David

Total number of authors:
20

Published in:
Toxicology and Applied Pharmacology

Link to article, DOI:
10.1016/j.taap.2014.12.011

Publication date:
2015

Document Version
Publisher's PDF, also known as Version of record

Toxicology and Applied Pharmacology 284 (2015) 16–32

Contents lists available at ScienceDirect

Toxicology and Applied Pharmacology

journal homepage: www.elsevier.com/locate/ytaap

MWCNTs of different physicochemical properties cause similar inflammatory responses, but differences in transcriptional and histological markers of fibrosis in mouse lungs

Sarah S. Poulsen [a,c,*], Anne T. Saber [a], Andrew Williams [b], Ole Andersen [c], Carsten Køhler [d], Rambabu Atluri [e], Maria E. Pozzebon [f], Stefano P. Mucelli [f], Monica Simion [g], David Rickerby [h], Alicja Mortensen [i], Petra Jackson [a], Zdenka O. Kyjovska [a], Kristian Mølhave [d], Nicklas R. Jacobsen [a], Keld A. Jensen [a], Carole L. Yauk [b], Håkan Wallin [a,j], Sabina Halappanavar [b], Ulla Vogel [a,d]

[a] National Research Centre for the Working Environment, Copenhagen DK-2100, Denmark
[b] Environmental and Radiation Health Sciences Directorate, Health Canada, Ottawa, Ontario K1A 0K9, Canada
[c] Department of Science, Systems and Models, Roskilde University, DK-4000 Roskilde, Denmark
[d] Department of Micro- and Nanotechnology, Technical University of Denmark, DK-2800 Kgs. Lyngby, Denmark
[e] Nanologica AB, SE-114 28 Stockholm, Sweden
[f] Veneto Nanotech SCpA, ECSIN — European Centre for the Sustainable Impact of Nanotechnology, I-45100 Rovigo, Italy
[g] Laboratory of Nanobiotechnology, National Institute for Research and Development in Microtechnologies, 077190 Bucharest, Romania
[h] European Commission Joint Research Centre Institute for Environment and Sustainability, I-21027 Ispra, VA, Italy
[i] National Food Institute, Technical University of Denmark, Søborg, Denmark
[j] Department of Public Health, University of Copenhagen, DK-1014 Copenhagen K, Denmark

ARTICLE INFO

Article history:
Received 13 October 2014
Revised 8 December 2014
Accepted 18 December 2014
Available online 29 December 2014

Keywords:
Nanotoxicology
In vivo
Toxicogenomics
DNA microarray
Acute phase response
ROS production

ABSTRACT

Multi-walled carbon nanotubes (MWCNTs) are an inhomogeneous group of nanomaterials that vary in lengths, shapes and types of metal contamination, which makes hazard evaluation difficult. Here we present a toxicogenomic analysis of female C57BL/6 mouse lungs following a single intratracheal instillation of 0, 18, 54 or 162 μg/mouse of a small, curled (CNT_{Small}, 0.8 ± 0.1 μm in length) or large, thick MWCNT (CNT_{Large}, 4 ± 0.4 μm in length). The two MWCNTs were extensively characterized by SEM and TEM imaging, thermogravimetric analysis, and Brunauer–Emmett–Teller surface area analysis. Lung tissues were harvested 24 h, 3 days and 28 days post-exposure. DNA microarrays were used to analyze gene expression, in parallel with analysis of bronchoalveolar lavage fluid, lung histology, DNA damage (comet assay) and the presence of reactive oxygen species (dichlorodihydrofluorescein assay), to profile and characterize related pulmonary endpoints. Overall changes in global transcription following exposure to CNT_{Small} or CNT_{Large} were similar. Both MWCNTs elicited strong acute phase and inflammatory responses that peaked at day 3, persisted up to 28 days, and were characterized by increased cellular influx in bronchoalveolar lavage fluid, interstitial pneumonia and gene expression changes. However, CNT_{Large} elicited an earlier onset of inflammation and DNA damage, and induced more fibrosis and a unique fibrotic gene expression signature at day 28, compared to CNT_{Small}. The results indicate that the extent of change at the molecular level during early response phases following an acute exposure is greater in mice exposed to CNT_{Large}, which may eventually lead to the different responses observed at day 28.

Abbreviations: BAL, bronchoalveolar lavage; BET, Brunauer–Emmett–Teller surface area analysis; CNT, carbon nanotube; COPD, chronic obstructive pulmonary disease; DCFH-DA, 2′,7′-dichlorofluorescein diacetate; FDR, false discovery rate; GO, gene ontology; Mitsui-7, Mitsui XNRi-7; MWCNT, multi-walled carbon nanotube; Nano-CB, nano-carbon black; SEM, Scanning Electron Microscopy; TEM, Transmission Electron Microscopy; TGA, thermogravimetric analysis.

* Corresponding author at: National Research Centre for the Working Environment, Lersø Parkallé 105, DK-2100 Copenhagen, Denmark.
E-mail addresses: spo@nrcwe.dk (S.S. Poulsen), ats@nrcwe.dk (A.T. Saber), Andrew.williams@hc-sc.gc.ca (A. Williams), oa@ruc.dk (O. Andersen), carko@nanotech.dtu.dk (C. Køhler), rba@nrcwe.dk (R. Atluri), mariaelena.pozzebon@yahoo.it (M.E. Pozzebon), stefano.pozzimucelli@venetonanotech.it (S.P. Mucelli), moni304ro@gmail.com (M. Simion), david.rickerby@jrc.ec.europa.eu (D. Rickerby), almo@food.dtu.dk (A. Mortensen), pja@nrcwe.dk (P. Jackson), zky@nrcwe.dk (Z.O. Kyjovska), kristian.molhave@nanotech.dtu.dk (K. Mølhave), nrj@nrcwe.dk (N.R. Jacobsen), kaj@nrcwe.dk (K.A. Jensen), Carole.yauk@hc-sc.gc.ca (C.L. Yauk), hwa@nrcwe.dk (H. Wallin), Sabina.halappanavar@hc-sc.gc.ca (S. Halappanavar), ubv@nrcwe.dk (U. Vogel).

http://dx.doi.org/10.1016/j.taap.2014.12.011

Introduction

Production and use of multi-walled carbon nanotubes (MWCNTs) have increased extensively over the last decade (Beg et al., 2011; Klumpp et al., 2006), thereby increasing the potential exposure for both workers and consumers. Exposure to MWCNT via inhalation, instillation or aspiration causes pulmonary effects in rodents including lung inflammation, sustained interstitial fibrosis, and granuloma formation (Ma-Hock et al., 2009; Pauluhn, 2010a; Pauluhn, 2010b; Porter et al., 2010; Reddy et al., 2010; Wang et al., 2011a).

MWCNTs vary in their length, wall thickness, aspect ratio, level and type of metal contamination, and surface chemistry, all of which are suggested to significantly influence their toxic potential. Thus, it is unclear if toxic responses observed after exposure to a specific MWCNT may be extrapolated in a general way to expected toxic potentials of other MWCNT types. It has been hypothesized that larger MWCNT, with a high length/diameter-aspect ratio, may resemble asbestos and be more carcinogenic and fibrogenic (Donaldson et al., 2010; Grosse et al., 2014). For example, intraperitoneal instillation of MWCNT of different lengths resulted in length-dependent infiltration of inflammatory cells in the peritoneal cavity of mice (Poland et al., 2008; Yamashita et al., 2010; Rittinghausen et al., 2014). Elevated inflammation, protein concentration, and fibrotic lesions along the parietal pleura and in the mesothelial layer were observed in mice exposed to long MWCNT via direct injection into the pleural cavity compared to mice exposed to short MWCNT. In contrast, responses to short MWCNT mirrored the responses of mice injected with control vehicle (Murphy et al., 2011). Thus, length and straightness play an important role in the toxicity induced by MWCNT. However, how these parameters influence the toxicity at the molecular level is unclear.

The objective of the present study was to employ toxicogenomics tools to systematically characterize the biological pathways and functions perturbed in mouse lungs exposed to two well-characterized OECD Working Party on manufactured Nanomaterials standard MWCNTs that differ in length, thickness, level of agglomeration and content of metal impurities, in order to identify mechanisms of toxicity that are distinctly associated with the two types of MWCNT. Genomic tools provide a unique means to globally profile all of the molecular pathways perturbed in response to MWCNT exposure, and thus permit detailed characterization and categorization of the potential health hazards of different MWCNTs. The expression profiles or perturbed biological pathways that are identified can then be used to build a property-response comparison, which contrasts the two different MWCNTs and their impact on gene expression, and thereby brings us closer to identifying biomarkers for human biomonitoring.

In the present study, groups of six female C57BL/6 mice were exposed by single intratracheal instillation to 18, 54 or 162 μg/mouse of small MWCNT NRCWE-026 (0.8 ± 0.1 μm in length) or large MWCNT NM-401(4 ± 0.4 μm in length). Due to the high likelihood of exposure of personnel during inhalation experiments, intratracheal instillation was used as a safe substitute for deposition through inhalation. Instillation is rapid, and the dose is easily controlled and reasonably well-distributed in the lung (Driscoll et al., 2000). Lung tissues from each group of mice were harvested 24 h, 3 d and 28 d after exposure. Global gene expression, inflammatory and genotoxic responses, lung morphology, as well as acellular production of free radicals were assessed to profile the pulmonary responses. Bioinformatics tools were used to compare and contrast the expression profiles.

Methods

Multiwalled carbon nanotubes

The following MWCNTs were used in the present study: The NRCWE-026 (Nanocyl NC7000 CNT, Sambreville, Belgium) a small/thin curled MWCNT referred to as CNT_{Small}. NM-401 is a larger/thick MWCNT (kindly donated by the European Union Joint Research Centre, Ispra, Italy) referred to as CNT_{Large}. Both MWCNTs are included in the OECD Working Party on Manufactured Nanomaterials. The length and diameter of both MWCNTs were measured in the Nanogenotox project and are shown in Table 1 (The Nanogentox group, 2013). CNT_{Large} is physicochemically similar to Mitsui XNRi-7 (in this study referred to as Mitsui-7), which has been classified as possibly carcinogenic to humans (Group 2B) (Grosse et al., 2014).

Dose selection.

Doses and time points were selected based on the previous and ongoing studies in our group (Bourdon et al., 2012b; Husain et al., 2013; Jacobsen et al., 2009; Poulsen et al., 2013; Saber et al., 2012, 2013). The consistency in doses and time points across many studies enabled comparison of responses after exposure to different nanomaterials. The doses reflect pulmonary deposition in mice after 1, 3, and 9 working days of 8 h at the Danish occupational exposure limit of 3.5 mg/m^3 for Printex90 carbon black particles (Bourdon et al., 2012b). Studies investigating personal exposure to CNT in occupational environments reported human exposure levels ranging from non-detectable up to 1 mg/m^3 (Methner et al., 2010; Dahm et al., 2013; Lee et al., 2014). However, most levels were in the range of 10–300 $\mu g/m^3$ (Hedmer et al., 2014; Han et al., 2008; Lee et al., 2010; Methner et al., 2012; Birch et al., 2011). Erdely et al. reported workplace exposure levels up to 10.6 $\mu g/m^3$, resulting in a calculated deposited dose of approximately 4.07 μg/day in a human, equivalent to 2 ng/day in the mouse (Erdely et al., 2013). Thus, although within dose ranges of other instillation/aspiration studies (Park et al., 2009; Porter et al., 2010; Shvedova et al., 2008; Snyder-Talkington et al., 2013), the doses used in present study are to be considered high in a workplace environment.

Preparation of instillation medium and exposure stock

CNTs were suspended by sonication in NanoPure water containing 2% serum collected from C57BL/6 mice. The particle suspensions (3.24 mg/ml) were sonicated using a Branson Sonifier S-450D (Branson Ultrasonics Corp., Danbury, CT, USA) equipped with a disruptor horn (Model number: 101-147-037). Total sonication time was 16 min at 40 W. During the sonication procedure the samples were continuously cooled on ice. Vehicle controls contained NanoPure water with 2% serum and were sonicated as described for the CNT suspensions.

Animal handling and exposure

Female C57BL/6 mice at the age of 5–7 weeks from Taconic (Ry, Denmark) were acclimatized for 1–3 weeks before the experiment. All mice were fed on Altromin (no. 1324, Christian Petersen, Denmark) and had access to water ad libitum during the whole experiment. The mice were housed in groups of up to 10 animals in polypropylene cages with sawdust bedding and enrichment at controlled temperature 21 ± 1 °C and humidity 50 ± 10% with a 12-h light/12-h dark cycle. At 8 week of age, groups of 9 C57BL/6 mice were exposed to 0, 18, 54 or 162 μg of CNT_{Small} or CNT_{Large} via intratracheal instillation (Jacobsen et al., 2009; Saber et al., 2012). Histological analyses and Transmission Electron Microscopy (TEM) were performed on 3 dedicated animals from each dose group. In brief, the mice were anesthetized with 4% isoflurane until fully relaxed and 2.5% during the instillation. Vehicle controls were intratracheally instilled with NanoPure water with 2% serum sonicated as described for the CNT suspensions. The mice were kept on their backs at a 40-degree angle during the entire procedure. The doses (18, 54 and 162 μg of CNT_{Small} or CNT_{Large}) were administered via a single intratracheal instillation. A 50 μl suspension was instilled followed by 150 μl air with a 250 μl SGE glass syringe (250F-LT-GT, MicroLab, Aarhus, Denmark). Control animals were instilled with vehicle (NanoPure water with 2% serum). After the instillation the catheter

Table 1
Physiochemical properties of CNT_{Small} and CNT_{Large}.

MWCNT	Code	Producer	CNT length (±SD)	CNT diameter (±SD)	BET (m^2/g)	Impurities (wt.%)
CNT_{Small}	NRCWE-026	Nanocyl (NC-7000)	0.85 ± 0.457 μm	11 ± 4.5 nm	245.8	13
CNT_{Large}	NM-401	IO-LE-TECNanomaterials (CP-0006-SG)	4.05 ± 2.40 μm	67 ± 26.2 nm	14.6	3

Data is obtained from analyses performed in the present study and in The Nanogentox group (2013).

was removed, breathing was observed in order to assure that the delivered material did not block the airways.

At 1, 3 or 28 days post-instillation, the mice were anesthetized by subcutaneous injection of 0.2 ml of Hypnorm® (fentanyl citrate 0.315 mg/ml and fluanisone 10 mg/ml, Janssen Pharma) and Dormicum® (Midazolam 5 mg/mL, Roche) in sterile water and killed by exsanguination via intracardiac puncture.

All animal procedures followed the guidelines for the care and handling of laboratory animals established by Danish laws and regulations. The Animal Experiment Inspectorate under the Ministry of Justice approved the study (#2010/561-1779).

BAL fluid and tissue collection

Immediately after withdrawing the heart blood, bronchoalveolar lavage (BAL) was performed on 6 mice in each dose group by lavaging the lungs twice using (1 ml/25 g body weight) saline water in a 1 or 2 ml syringe. Each lavage consisted of 3 up and down movements performed slowly (5–10 s each). The second lavage was performed with fresh saline water. Both washings were immediately put on ice. The combined lavage volume recovered was estimated and BAL fluid and BAL cells were separated by centrifugation at 4 °C and 400 g for 10 min. The BAL cell pellet was resuspended in 170 μl medium (HAMS F12 (GIBCO #21765) with 10% FBS) and stored at −80 °C. The lavaged lung lobes were removed and snap-frozen in cryotubes in liquid N_2 and stored at −80 °C for later microarray and qRT-PCR experiments. For TEM imaging, the lungs were fixed in situ by cannulating the trachea and delivering 2% glutaraldehyde in 0.05 M cacodylate buffer (pH 7.2) at a constant fluid pressure of 30 cm before the thorax was opened. The fixative was mixed from glutaraldehyde (SPI 230 Supplies #02608) and sodium cacodylate (Sigma-Aldrich #C4945). Thereafter, the lungs were excised and immersed in 2% glutaraldehyde 0.05 M cacodylate buffer (pH 7.2) and stored at 5 °C until further processing. For the histological examination, the fixed lungs from two randomly selected animals from the vehicle control and the high-dose CNT_{Small} or CNT_{Large} groups were embedded in paraffin, sectioned in 4–6 μm sections and stained with hematoxylin and eosin (HE) or trichrome for histological examination.

Bronchoalveolar lavage cell counts

For determination of bronchoalveolar lavage (BAL) cell composition, cells in 50 μl suspension were collected on microscope slides by centrifugation at 10,000 rpm for 4 min in a Cytofuge 2 (StatSpin, Bie and Berntsen, Rødovre, Denmark). The slides were fixed with 96% ethanol and stained with May–Grünwald–Giemsa stain. The cell type composition of BAL was determined on 200 cells and the total number of cells was determined by the Nucleo Counter (Chemometec, Allerød, Denmark) Live/dead assay according to the manufacturer's instructions.

The statistical analyses on BAL cell counts were performed in SAS version 9.3 (SAS Institute Inc., Cary, NC, USA). With the exception of day 28 for lymphocytes, no differences in controls at the separate days were identified and they were pooled. We decided to pool the lymphocyte controls in order to maintain consistency. Statistical significance was calculated using a parametric two-way ANOVA with a post-hoc Tukey-type experimental comparison test. In case of interaction between dose and time, the data was separated in time points and a one-way ANOVA with a post-hoc Tukey-type experimental comparison test was performed. In cases when the data, after log transformation, did not meet the parametric requirements, non-parametric tests were used.

Thermal gravimetric analysis

Thermal gravimetric analysis (TGA) determines the weight loss of a material as a function of temperature whilst derivative thermal gravimetric analysis (DTG) gives rate of change of mass. From a TGA curve it is possible to determine the mass % of organic content and to determine the thermal stability of the samples. TGA was performed on a Perkin TGA instrument for (CNT_{Small}) and a Mettler TGA (for CNT_{Large}). The samples were heated from 25 to 950 °C at a heating rate of 10 °C/min on an alumina holder under the flow of air of 20 ml/min.

Brunauer–Emmett–Teller (BET) surface area analysis

The samples were degassed under vacuum for 10 h at 80 °C and nitrogen absorption isotherms were measured at liquid nitrogen temperature (77 K) using a Micromeritics ASAP2020 volumetric adsorption analyzer. The Brunauer–Emmett–Teller equation was used to calculate the surface area from adsorption data obtained in the relative pressure (p/po) range of 0.05 and 0.3. The total pore volume was calculated from the amount of gas adsorbed at p/po = 0.99. Pore size distribution curves were derived using Barrett–Joyner–Halenda (BJH) assuming a cylindrical pore model.

Light microscopy

One micrometer semi-sections of embedded lung were cut with a Zeiss Ultracut UCT ultra-microtome, stained with 1% toluidine blue in 1% borax and imaged using a Zeiss AxioImager Z1 widefield microscope.

Scanning Electron Microscopy

Five microliters of CNT_{Small} or CNT_{Large} in exposure medium was deposited on an Al foil covered Scanning Electron Microscopy (SEM) stub. The size and agglomeration was determined by SEM using a NVISION 40 Zeiss Cross-Beam Focused Ion Beam machine, operated at 10 kV accelerating voltage, equipped with a high resolution Gemini Field Emission Gun scanning electron microscope column and with an Oxford INCA 350 Xact Energy Dispersive X-Ray Spectrometer having an energy resolution of 129 eV at the Mn kα line.

Transmission Electron Microscopy

Pristine MWCNT and lung sections from mice exposed to CNT_{Small} or CNT_{Large} were visualized using TEM. The fixed lung was cut into small pieces and a standard Electron Microscope embedding procedure was carried out as described in Kobler et al. (2014). Samples were rinsed in 0.15 M phosphate buffer followed by a 0.15 M sodium cacodylate wash. Post-fixation and osmofication were performed in 2% osmium tetroxide in 0.05 M potassium ferricyanide for 2 h. After osmofication, samples were rinsed in deionized water and placed in 1% uranyl acetate in water overnight at 5 °C. The following day samples were gradually dehydrated in ethanol and lastly in propylene oxide. Embedding was

performed in propylene oxide diluted Epon, until 100% Epon 812 was used before polymerization at 60 °C for 24 h. Samples were cut into approximately 80 nm sections for TEM using an ultramicrotome with a diamond knife. Sections were stained with uranyl acetate and lead citrate, and imaged using a CM 100 BioTwin instrument from Philips operated at 80 kV accelerating voltage.

Microarray experiment

Total RNA extraction for microarray analysis.
Total RNA was isolated from lung tissue of 144 mice in total (n = 6 mice per dose group). TRIzol reagent (Invitrogen, Carlsbad, CA, USA) was used for RNA isolation and purification was done using the RNeasy MiniKit (Qiagen, Mississauga, ON, Canada) as specified by the manufacturer. An on-column DNase treatment was applied (Qiagen, Mississauga, ON, Canada). All RNA samples showing A260/280 ratios between 2.0 and 2.15 were further analyzed for RNA integrity using an Agilent 2100 Bioanalyzer (Agilent Technologies, Mississauga, ON, Canada). Only RNA with integrity numbers above 7.0 was used in the microarray hybridization experiment. All RNA samples (6 per group) passed the quality control. Total RNA was stored at −80 °C until analysis (Husain et al., 2013; Poulsen et al., 2013).

Hybridization.
Microarray hybridization was performed using 200 ng total RNA from each sample (n = 6 per group) on Agilent 8 × 60 K oligonucleotide microarrays (Agilent Technologies Inc., Mississauga, ON, Canada) as described previously (Poulsen et al., 2013). Data were acquired using Agilent Feature Extraction software version 9.5.3.1.

Statistical analysis of microarray data.
A reference randomized block design (Kerr, 2003; Kerr and Churchill, 2007), with the sample labeled with Cy5 and the reference labeled with Cy3, was used to analyze gene expression microarray data. LOcally WEighted Scatterplot Smoothing (LOWESS) (Cleveland, 1979) regression modeling method was used to normalize data and statistical significance of the differentially expressed genes was determined using MicroArray ANalysis Of VAriance (MAANOVA) (Wu et al., 2003) in R statistical software (http://www.r-project.org). The Fs statistic (Cui et al., 2005), a shrinkage estimator for the gene-specific variance components, was used to test the treatment effects. The permutation method (30,000 permutations with residual shuffling) was used to estimate the P-values for all the statistical tests, and these P-values were then adjusted for multiple comparisons by using the false discovery rate multiple testing correction (Benjamini and Hochberg, 1995). Fold change calculations were based on the least-square means. Genes showing expression changes of at least 1.5 fold in either direction compared to their matched controls and having P-values of less than or equal to 0.05 ($P \leq 0.05$) were considered as significantly differentially expressed and were used in the downstream analysis.

Functional and pathway analysis of differentially expressed genes.
The Database for Annotation, Visualization and Integrated Discovery (DAVID) v6.7 (Huang et al., 2009a,b) was used for the functional Gene Ontology (GO) analysis of the differentially expressed genes. Benjamini–Hochberg corrected GO biological processes with a Fisher's exact $P \leq 0.05$ were considered to be significantly enriched. Specific biological functions, pathways and networks associated with the differentially expressed genes were identified using Ingenuity Pathway Analysis (IPA, Ingenuity Systems, Redwood City, CA, USA). Functions, pathways and networks with a Benjamini–Hochberg Multiple Testing Correction P-value of ≤0.05 were considered for discussion. The pathway analysis methods employed enabled the extraction of biologically meaningful information from a long list of differentially expressed genes.

qRT-PCR validation

For validation of microarray results, 8 genes were evaluated by qRT-PCR at all doses and time points. These genes (*Saa3*, *Il1α*, *Il6*, *Cxcl2*, *Ccl2*, *Hmox1*, *Mmp9* and *Sod2*) showed high differential regulation at a minimum of one dose or time point, and were involved in inflammation, acute phase response, protection from ROS or extracellular matrix remodeling.

Total RNA extraction for qRT-PCR validation.
Total RNA was isolated from lung tissue of 144 mice in total (n = 6 mice per dose group) using the MagNA Pure Compact RNA Isolation kit (Roche) according to the manufacturer's protocol. In brief, the RNA isolation procedure is based on the MagNA Pure Magnetic Glass Particle (MGP) Technology (Roche): nucleic acids are bound on the surfaces of MGPs whereas unbound molecules are removed by several washing steps. Genomic DNA molecules are degraded by incubation with DNase. Total RNA was stored at −80 °C until analysis.

cDNA synthesis.
cDNA synthesis was performed using the Enhanced Avian HS RT-PCR kit (Sigma-Aldrich), with total RNA as template, as described in the manufacturer's protocol. A total of 500 ng was used for each cDNA synthesis. The heating cycle was 25 °C (15 min)/50 °C (50 min)/85 °C (5 min) and the obtained cDNA solutions were further diluted to a final concentration of 10 ng/μl.

Real-time RT-PCR.
The expression of the target genes, compared to a reference (GAPDH), was determined with real time-PCR using a LightCycler® 480 Instrument (Roche) according to the manufacturer's protocol. The relative expression was calculated using the Livak–Schmittgen method (Livak and Schmittgen, 2001). The statistical analyses were performed in Microsoft Excel through Mathematica (version 8, Wolfram Research). Statistical significance was calculated using a parametric one-way ANOVA. Regression analysis between PCR and microarray data was performed in SAS version 9.3 (SAS Institute Inc., Cary, NC, USA).

ROS generating ability using dichlorodihydrofluorescein

The generation of ROS was assessed using 2′,7′-dichlorofluorescein diacetate (DCFH-DA) (Invitrogen) as previously described by Jacobsen et al. (2008). CNT_{Small} and CNT_{Large} suspensions were prepared with Hank's buffered saline solution instead of serum at doses: 0, 1.4, 2.8, 5.6, 11.3, 22.5, 45, 90 and 135 μg/ml.

Comet analysis

The comet analysis was performed on lung tissue based on a previously published protocol (Jackson et al., 2011a), which has been modified and validated to a fully-automated scoring system (IMSTAR). This new procedure for scoring DNA damage, quantified as %DNA in tail and tail length, has recently been published (Jackson et al., 2013). The statistical analyses were performed in SAS version 9.3 (SAS Institute Inc., Cary, NC, USA). No differences in controls at the separate days were identified and they were pooled. After careful evaluation, 3 control samples were excluded due to unusually high levels of DNA strand breaks and apoptotic cells. This is likely due to incorrect thawing procedure, as previously described in Jackson et al. (2013). One belonged to the day 3 control group, the last 2 belonged to the 28 days group. Statistical significance was calculated using a parametric two-way ANOVA with a post-hoc Tukey-type experimental comparison test. In case of interaction between dose and time, the data was separated in time points and a one-way ANOVA with a post-hoc Tukey-type experimental comparison test was performed. In cases where the data, after log

transformation, did not meet the parametric requirements, non-parametric tests were used.

Results

Mice were exposed by intratracheal instillation to three different doses (18, 54 and 162 μg/mouse) of two MWCNTs: CNT_{Small} (NRCWE-026) and CNT_{Large} (MWCNT NM-401), alongside vehicle controls. Lung tissue was collected 1, 3 and 28 days after the exposure.

MWCNT characteristics

Table 1 summarizes the physicochemical characterization data.

CNT_{Small}

The average length of CNT_{Small} was 0.85 ± 0.46 μm (mean ± SD) and the average width was 11 ± 4.5 nm (mean ± SD) (Kobler et al., 2014; The Nanogentox group, 2013). The CNT_{Small} was stable up to 400 °C in thermogravimetric analysis (TGA), and at 800 °C, 13% of the mass still remained (Supplementary Fig. 1.A), most likely metal oxides since chemical analysis of CNT_{Small} from the same batch by Jackson et al. (2014) showed that the reported main components of CNT_{Small} (NRCWE-026) include: C (84.4%), Al_2O_3 (14.97%), Fe_2O_3 (0.29%) and CoO (0.11%). The Brunauer–Emmett–Teller surface area (BET) of CNT_{Small} was 245.8 m^2/g, most of this being micro-pores.

The pristine CNT_{Small} was visualized using Transmission Electron Microscopy (TEM). The pristine nanotubes appeared curly, varied in their lengths (Supplementary Figs. 2.A–B), and both agglomerated and single CNT_{Small} were observed. In their agglomerated state, the CNT_{Small} appeared highly entangled and the single tube-like structure was no longer visible. Scanning Electron Microscopy (SEM) of CNT_{Small} in the exposure medium revealed mainly agglomerated and entangled MWCNTs (Fig. 1.A). Impurities and protein matter from the exposure medium were observed throughout the samples, probably originating from contamination during synthesis and from the dried exposure medium.

Light microscope images of CNT_{Small} in the alveolar region showed uniform dispersion and distribution of CNT_{Small} on day 1 after the exposure to 162 μg (Fig. 1.C). TEM analysis of interactions between

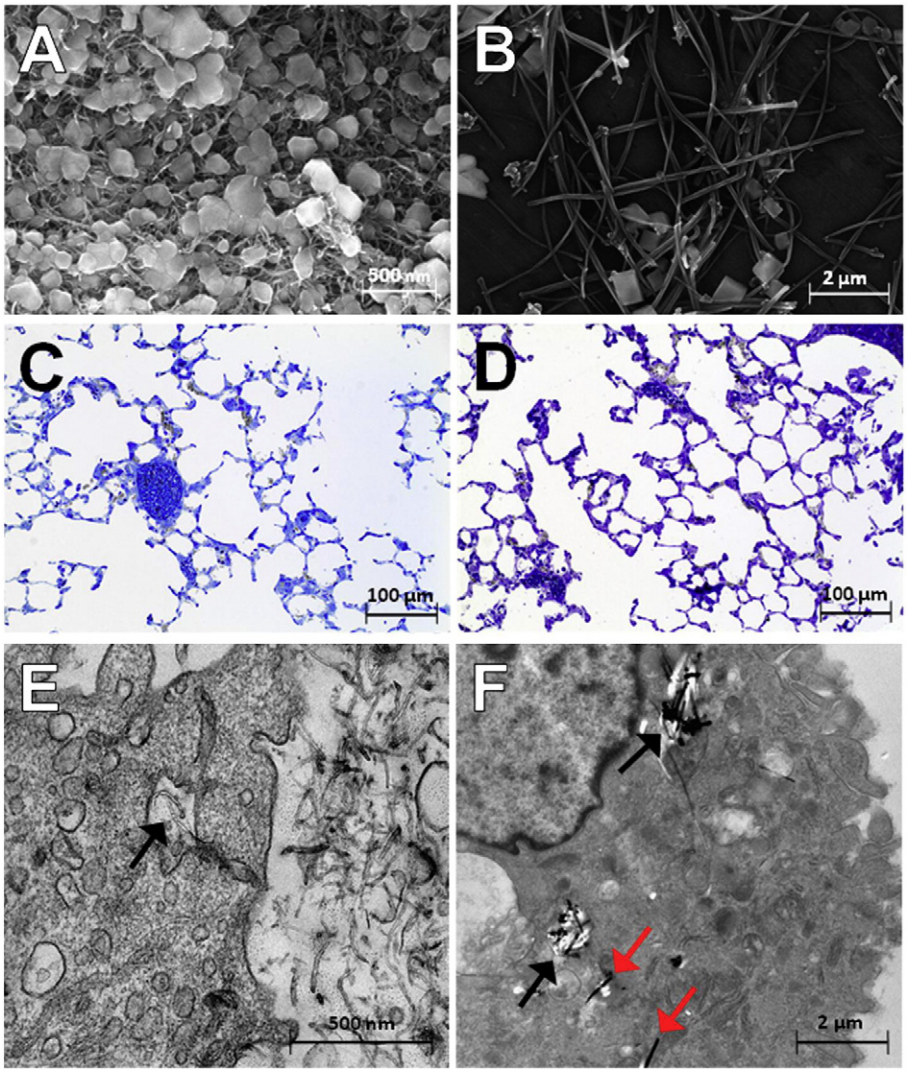

Fig. 1. Microscopy imaging of CNT_{Small} and CNT_{Large}. (A) SEM image of CNT_{Small} in instillation medium. The impurities and protein matter may originate from the dried instillation medium. (B) SEM image of CNT_{Large} in instillation medium. The impurities and salt crystals observed probably originate from the dried instillation medium. (C) and (D) are light microscopy images of the alveolar lumen 1 day after exposure at dose 162 μg to CNT_{Small} and CNT_{Large}, respectively. (E) TEM image of CNT_{Small} interacting with cells of the lung lining 3 days after exposure to 162 μg CNT_{Small}. CNT_{Small} engulfed in vesicles (black arrow) were observed. (F) TEM image of CNT_{Large} interacting with a cell with morphological traits of a macrophage 3 days after exposure to 162 μg CNT_{Large}. CNT_{Large} was observed both as engulfed in vesicles (black arrow) and as free CNT_{Large} in the cytoplasm (red arrow).

CNT_{Small} and cells in the lung lining at post-exposure day 3 (Fig. 1.E and Supplementary Fig. 2.C) showed curled and agglomerated CNT_{Small} engulfed in vesicles in the cytoplasm.

CNT_{Large}

The average length of CNT_{Large} was 4.05 ± 2.4 μm (mean ± SD) and the average width was 67 ± 26.2 nm (mean ± SD) (Kobler et al., 2014; The Nanogentox group, 2013) (Table 1). Based on the standard deviation, 5% of the CNT_{Large} tubes are larger than 8847.8 nm. TGA showed stability of the CNT_{Large} sample until 650 °C. The total carbon was decomposed between 650 and 950 °C, leaving a mass of 3% after a complete decomposition (Supplementary Figs. 1.B–C). The chemical composition of CNT_{Large} from the same batch has been determined by Jackson et al. (2014). The reported main components of CNT_{Large} (NM-401) included: C (99.7%), P_2O_5 (0.14%), CO_3 (0.08%) and Fe_2O_3 (0.05%). The CNT_{Large} sample had a low volume of N_2 adsorption under a relative pressure of 0.3, which implies that the sample possessed a small (14.6 m^2/g) non-porous surface area.

TEM imaging of the pristine CNT_{Large} revealed MWCNT that appeared long and straight (Supplementary Figs. 3.A–B). Different levels of agglomeration were observed, but monomers of CNT_{Large} were visible in the bundle and were straight. SEM of CNT_{Large} in the exposure medium (Fig. 1.B) showed long and straight CNT_{Large} in tangled up bundles with a majority of them being longer than 1 μm. The observed spherical particles probably originated from the dried exposure medium.

Light microscope imaging of the alveolar region showed well dispersed CNT_{Large} in the entire region (Fig. 1.D). TEM imaging of the lung lining clearly showed CNT_{Large} interacting with macrophage-like cells (Fig. 1.F and Supplementary Fig. 3.C). A close-up of the cytoplasm revealed both single and bundles of CNT_{Large} within vesicles. Some of these vesicles appeared to be penetrated by the CNT_{Large}. In addition, visible damage caused by CNT_{Large} displacement and wear of the microtome diamond knife was observed. Such displacement and damage was not observed with the CNT_{Small} (Kobler et al., 2014).

Bronchoalveolar lavage fluid cell type composition

BAL fluid collected from MWCNT-instilled mice 1, 3 and 28 days after exposure was used to assess the recruitment of inflammatory cells into the lung lumen. The total numbers of cells, neutrophils, macrophages, eosinophils and lymphocytes cells are shown in Supplementary Table 1. For both MWCNTs, the inflammatory response was dominated by large infiltrations of neutrophils. The largest total influx of neutrophils was seen on post-exposure day 3, but the highest % of neutrophils in the total BAL fluid cells was observed at day 1 (Fig. 2). Persistent increases in neutrophil levels were observed up to 28 days post-exposure. For CNT_{Small} instilled mice, the neutrophil numbers at the 162 μg dose were 80.1 × 10^3 cells, 457 × 10^3 cells more than controls and 34.2 × 10^3 cells on post-exposure days 1, 3 and 28, respectively (Supplementary Table 1). Whereas, following high dose CNT_{Large} exposure the neutrophil numbers were 108.6 × 10^3 cells, 158.1 × 10^3 cells and 77.4 × 10^3 cells more than in controls on post-exposure days 1, 3 and 28, respectively (Supplementary Table 1). Overall, the cell type compositions of BAL were similar after exposure to the two MWCNTs, except for the eosinophil influx, which, especially at day 28, was higher in response to CNT_{Large}. Similar to an earlier Mitsui-7 study (Poulsen et al., 2013), an inverse dose–response relationship was observed for eosinophils. A similar trend was observed at day 3 for total number of lymphocytes. The great reduction in eosinophils and lymphocytes at the higher doses compared to the 18 μg dose has been addressed in our earlier publication (Poulsen et al., 2013).

Pulmonary gene expression analysis after exposure to CNT_{Small} and CNT_{Large}

Overview of the expression changes

Complete DNA microarray results for CNT_{Small} and CNT_{Large} exposures are available through the Gene Expression Omnibus at NCBI (http://www.ncbi.nlm.nih.gov/geo/, accession number: GSE35284). We identified 6639 unique differentially expressed genes represented by 9270 probes (false discovery adjusted $P < 0.05$ and the relative change in expression (fold change) was at least ±1.5 in either direction) after CNT_{Small} exposure, and 5972 genes represented by 8450 probes after CNT_{Large} exposure (Supplementary Table 2). These represent genes that were significantly different from control in at least one dose or time point for either CNT type. For both MWCNTs, a clear dose–response was observed at all time points. A time-dependency was observed with a peak at day 3 (Fig. 3). We tabulated the number of differentially regulated genes for CNT_{Small} for the three different post-exposure time points. On day 1, a total of 197 genes (117 down-regulated and 80 up-regulated), 848 genes (404 down-regulated and 444 up-regulated) and 2186 genes (1157 down-regulated and 1029 up-regulated) were differentially expressed in the 18, 54 and 162 μg dose groups, respectively (Fig. 3.A). On day 3, a total of 652 genes (193 down-regulated and 459 up-regulated), 2059 genes (866 down-regulated and 1193 up-regulated) and 5275 genes (2713 down-regulated and 2562 up-regulated) were differentially expressed in the 18, 54 and 162 μg dose groups, respectively (Fig. 3.B). On day 28, a total of 17 genes (3 down-regulated and 14 up-regulated), 37 genes (12 down-regulated and 25 up-regulated) and 111 genes (5 down-regulated and 106 up-regulated) were differentially expressed in the

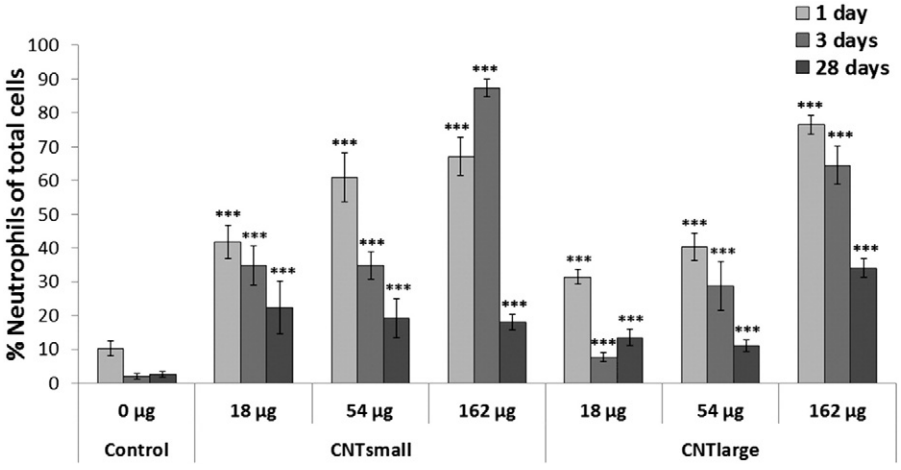

Fig. 2. Neutrophil levels in % of the total BAL fluid cells following exposure to CNT_{Small} and CNT_{Large}. Values for MWCNT exposed mice are mean of 5–6 mice. The values for vehicle instilled mice are mean of 24–25 mice. Error bars denote SEM. ***Statistically significantly different from vehicle instilled mice, $P < 0.001$.

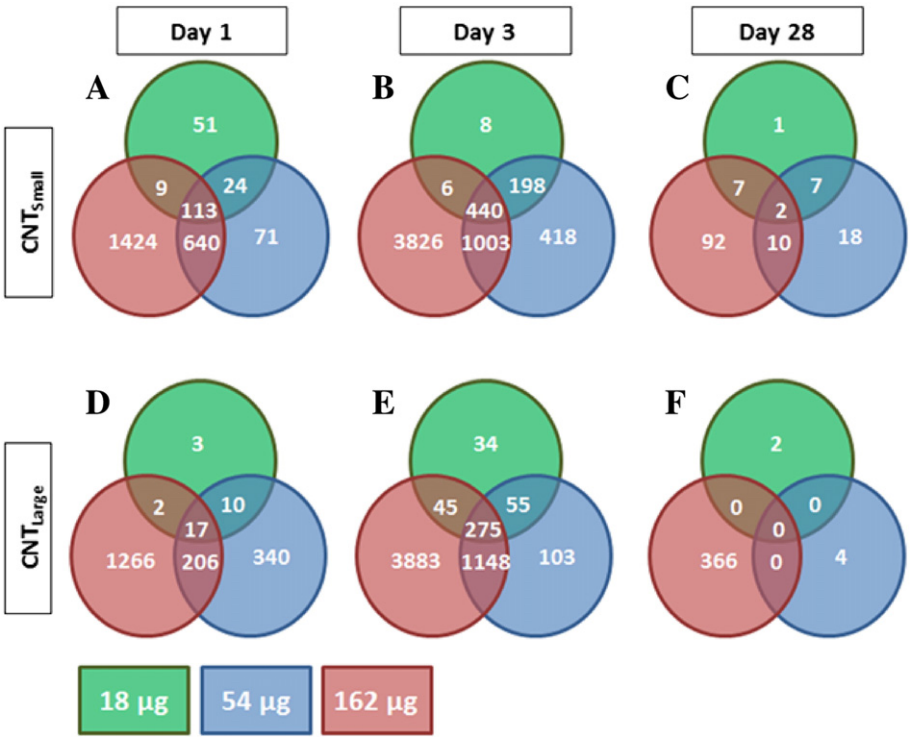

Fig. 3. Total number of differentially expressed genes ($P < 0.05$ and fold change ± 1.5). Green: Low dose (18 µg). Blue: Medium dose (54 µg). Red: High dose (162 µg). (A) CNT_{Small} at day 1. (B) CNT_{Small} at day 3. (C) CNT_{Small} at day 28. (D) CNT_{Large} at day 1. (E) CNT_{Large} at day 3. (F) CNT_{Large} at day 28.

18, 54 and 162 µg dose groups, respectively (Fig. 3.C). The number of differentially regulated genes following CNT_{Large} exposure on day 1 was a total of 32 genes (8 down-regulated and 24 up-regulated), 573 genes (189 down-regulated and 384 up-regulated) and 1491 genes (729 down-regulated and 762 up-regulated) in the 18, 54 and 162 µg dose groups, respectively (Fig. 3.D). On day 3, a total of 409 genes (153 down-regulated and 256 up-regulated), 1581 genes (669 down-regulated and 912 up-regulated) and 5351 genes (2798 down-regulated and 2553 up-regulated) were differentially expressed in the 18, 54 and 162 µg dose groups, respectively (Fig. 3.E). On day 28, a total of 2 genes (2 down-regulated and 0 up-regulated), 4 genes (2 down-regulated and 2 up-regulated) and 366 genes (89 down-regulated and 277 up-regulated) were differentially expressed in the 18, 54 and 162 µg dose groups, respectively (Fig. 3.F). A direct comparison of the total number of genes regulated in lung tissue after exposure to CNT_{Small} and CNT_{Large}, respectively, is shown in Supplementary Fig. 4. At the high dose exposure on post-exposure day 3, there was a high concordance between the genes differentially expressed after exposure to the two MWCNTs. At the lower doses and other time points, we observed less than 50% overlapping genes between the two groups. Differentially expressed genes following exposure to the high dose of CNT_{Large} were 4 times higher than CNT_{Small} on day 28, which may indicate a more sustained toxic response resulting from exposure to long, thick and straight MWCNT.

Gene ontology analysis of biological processes

In order to identify themes in the global pulmonary gene expression patterns caused by the two MWCNTs, we employed gene ontology (GO) classification through the Database for Annotation, Visualization and Integrated Discovery (DAVID) (Huang et al., 2009b,a). The common and unique biological processes affected by CNT_{Small} and CNT_{Large} are shown in Supplementary Figs. 5–7.

On post-exposure day 1 we identified two overlapping biological processes perturbed following exposure to CNT_{Small} and CNT_{Large}: defense response [GO:0006952] and cell motion [GO:0048870]. This indicates that inflammation and cell motility are common responses following exposure to CNTs at post-exposure day 1 and that they are not influenced by length or metal contaminants. Five unique biological processes were identified following high dose CNT_{Small} exposure on post-exposure day 1 (Supplementary Fig. 5.A), whereas exposure to CNT_{Large} resulted in unique enrichment of two biological processes at the medium and the high dose, and regulation of nine processes uniquely enriched at the high dose only (Supplementary Fig. 5.B). Although a higher prevalence of perturbed biological processes was observed following CNT_{Large} exposure compared to CNT_{Small} at post-exposure day 1, they mainly grouped in similar categories: Inflammatory response, cell motility and cell cycle processes. However, the biological process involving cell death was only perturbed after CNT_{Large} exposure (Supplementary Fig. 5.B). Similarly, at 3 days post-exposure, high concordance in enriched GO biological processes was observed following CNT_{Small} and CNT_{Large} exposure, with seven overlapping processes identified: cell cycle [GO:0007049], immune response [GO:0006955], defense response [GO:0006952], DNA metabolic process [GO:0006259], cytoskeleton organization [GO:0007010], microtubule-based process [GO:0007017], and cell activation [GO:0001775]. Exposure to CNT_{Small} also resulted in unique enrichment of 10 biological processes across the dose range at post-exposure day 3 (Supplementary Fig. 6.A), whereas four uniquely regulated processes were identified following CNT_{Large} exposure (Supplementary Fig. 6.B). Similar to the responses seen at post-exposure day 1, these unique biological processes primarily grouped under the same categories; inflammatory response, cell motility and cell cycle processes. However, in contrast to post-exposure day 1, we noted a unique regulation of cell death following exposure to CNT_{Small} at post-exposure day 3. On post-exposure day 28, no overlapping GO biological processes were observed following CNT_{Small} and CNT_{Large}. Immune response [GO:0006955] was perturbed at both low and medium doses following exposure to CNT_{Small} (Supplementary Fig. 7.A); whereas, perturbations in response to wounding [GO:0009611], ribonucleoside triphosphate metabolic process

[GO:0009199] and hydrogen transport [GO:0006818] (Supplementary Fig. 7.B) were observed at the high dose following CNT_{Large} exposure. This indicates a common sustained inflammatory response that persists until post-exposure day 28 following exposure to both CNT_{Small} and CNT_{Large}. In addition to the general observations of high similarities in perturbed GO biological processes, we also noted that CNT_{Small} exposure altered expression of genes involved in cell cycle and microtubule assembly, indicative of cell cycle arrest and structural damage at post-exposure day 1. Instead, CNT_{Large} exposure resulted in activation of immune responses, suggesting that the immediate responses to the two types of nanotubes are different and that there is a delay in the onset of immune responses following exposure to CNT_{Small}.

Property-response comparison

From the overall analysis of perturbed biological processes identified through GO, we constructed a property-response comparison of the five most perturbed biological processes: cell cycle [GO:0007049], immune response [GO:0006955], response to wounding [GO:0009611], DNA metabolic process [GO:0006259] and microtubule-based process [GO:0007017] (Fig. 4). This allowed us to identify the specific expression changes associated with selected ontologies across the two types of CNTs. In order to identify effects related to the physicochemical properties of CNT_{Large}, we organized the genes in the biological processes based on their expression following exposure to high dose of CNT_{Large} at post-exposure day 3. A high concordance was found between the differentially regulated genes in all five biological processes in response to both CNT types especially at the early time points. Underlying this observation is the low number of oppositely regulated genes observed. Minor differences in the potency of CNT_{Small} and CNT_{Large} on gene expression were noted in immune response and response to wounding at the high dose on day 3. Although similar genes were affected, these genes were more strongly induced or repressed following CNT_{Large} exposure. This indicates effects related specifically to the physicochemical properties of CNT_{Large}. However, at the low dose at post-exposure day 3,

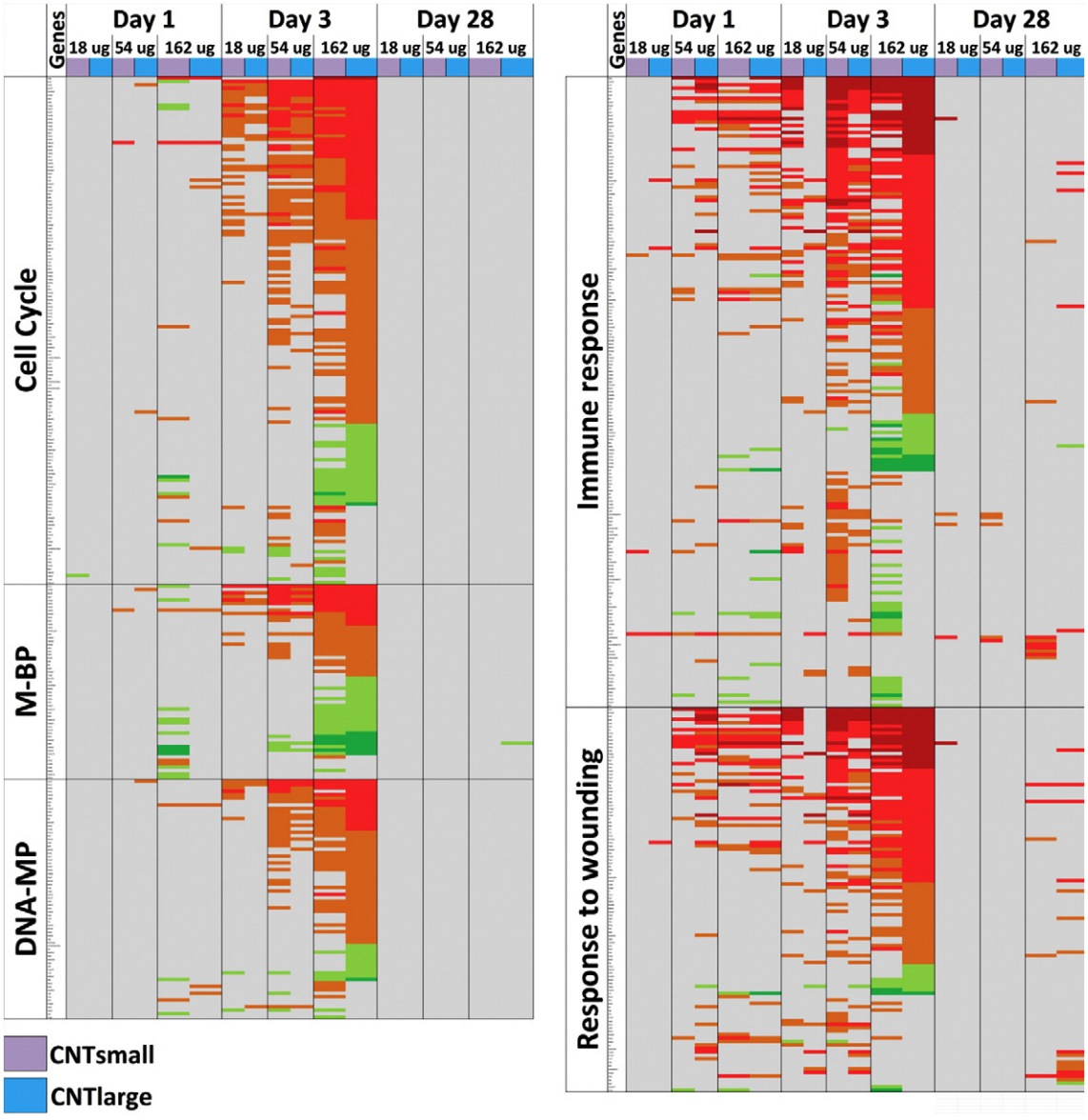

Fig. 4. Property-response comparison. Change in the expression of genes in five highly regulated selected GO biological processes relative to control mice. The genes are organized by the size of changes in expression after exposure to CNT_{Large} at the 162 μg dose at post-exposure day 3. GO biological processes selected: Cell cycle, microtubule-based process (M-BP), DNA metabolic process (DNA-MP), immune response and response to wounding. Significant ($P < 0.05$) gene expression color coding: Light green: Fold change between −2.999 and −2. Dark green: Fold change ≤ −3.000. Orange: Fold change between 2.000 and 2.999. Red: Fold change between 3.000 and 9.999. Dark red: Fold change ≥ 10.000. Gray: Fold change between −1.999 and 1.999 or not significant expression.

a much higher proportion of genes were differentially expressed after CNT_{Small} exposure compared to CNT_{Large}. This could, in turn, indicate a greater effect of CNT_{Small} compared to CNT_{Large} at low doses. We identified a cluster of uniquely changed genes on day 28 after exposure to CNT_{Large} in response to wounding. This indicates a sustained or delayed effect specific for the physicochemical properties of CNT_{Large}. This cluster included the genes *Chi3l4*, *Slc7a2*, *Ccr2*, *Lipa*, *Olr1*, *LOC620515*, *Chi3l3*, *Proz*, *Tff1* and *Gp9*. There is little cohesion between these genes in the scientific literature, and no clear conclusion can be drawn based on the cluster at this time.

Functional analysis

The functional significance of the GO changes was determined using Ingenuity Pathway Analysis (IPA) (Ingenuity® Systems, www.ingenuity.com). The individual enriched functions in IPA were filtered by: 1) removing redundant functions with overlapping genes, and 2) removing functions that were not directly relevant to the present study (e.g. dermal diseases and ophthalmic diseases). In general, we observed high similarities between the enriched functions across time point and doses, which confirm the results of the GO analysis of biological processes. The top five most significantly affected high-level functions after CNT_{Small} or CNT_{Large} exposure are shown in Fig. 5. These top changing functions only differed by one function: 'Inflammatory response' (CNT_{Large}) and 'hematological system, development and function' (CNT_{Small}). A closer analysis revealed that the function 'hematological system, development and function' was associated with annotation of terms such as "activation of leukocytes" and "migration of phagocytes", indicating that the enrichment of this biological function was based on the differential regulation of inflammatory genes. For both MWCNTs, analysis of the genes differentially expressed under these top five functions revealed significant impact on processes involved in the immune and acute phase response, especially regarding 'hematological system, development and function', 'inflammatory response' and 'cellular movement'. Indeed, changes in the mRNA levels of several chemokine (C–C motif) ligands (CCLs), chemokine (C–X–C motif) ligands (CXCLs), serine protease inhibitors (SERPINs), tumor necrosis factor family genes and acute phase genes, e.g. the serum amyloid A proteins (SAAs), were identified in all of the perturbed functions. Several of these genes were among the most up-regulated overall, but common for these were also that the changes in expression occurred at the early time points and were not sustained up to 28 days. Supplementary Table 3 lists the most differentially expressed genes at every time point and dose. A commonality for many of these genes is their involvement in the immune and acute phase responses. Serum amyloid A 3 (*Saa3*), a well characterized acute phase gene, had the largest fold change of all genes after exposure to both MWCNTs, peaking at 297-fold above controls on day 3 for the medium dose of CNT_{Small} and at 184-fold for the high dose on day 3 for CNT_{Large} (Supplementary Table 3). Looking beyond the top changing functions, we observed a difference in the expression of genes involved in 'free radical scavenging' (Supplementary Fig. 8). Exposure to CNT_{Large}, but not CNT_{Small}, resulted in altered expression of genes belonging to this function at the earliest time point. However, by day 3, this function was similarly enriched for both MWCNTs. Similar differences in the kinetics and delayed onset were also observed with immune response following CNT_{Small}.

Pathway analysis

The pathways with the largest number of differentially expressed genes caused by exposure to the high dose of CNT_{Small} and CNT_{Large} are shown in Table 2 for all time points. The pathway analysis was conducted in IPA. A general high overlap of perturbed pathways was observed across CNT_{Small} and CNT_{Large} exposure. On post-exposure day 1, LXR/RXR activation, atherosclerosis signaling, and acute phase response signaling were highly regulated following exposure to both MWCNTs, indicating important effects of MWCNT exposure on lipid/cholesterol homeostasis and the inflammatory response. The same trend for high concordance was observed on post-exposure day 3, with hepatic fibrosis/hepatic stellate cell activation and dendritic cell maturation regulated across both MWCNT types. Although the other significantly enriched pathways differed from CNT_{Small} to CNT_{Large} exposure, they commonly involved lipid/cholesterol homeostasis and the inflammatory response, thus linking to the response seen at the early time point. Based on this

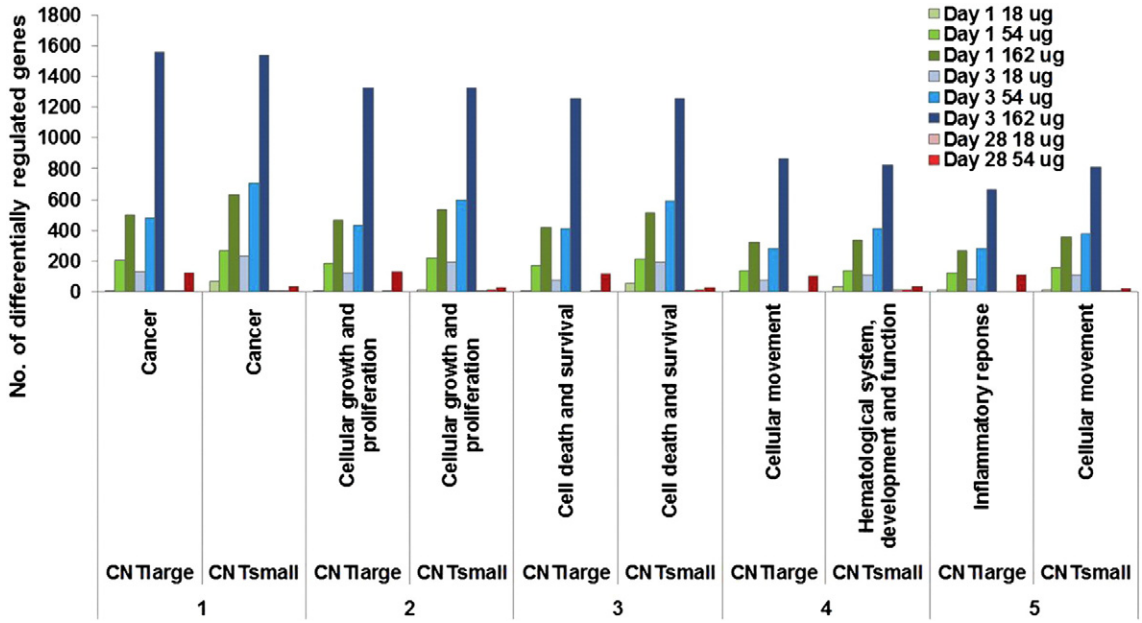

Fig. 5. Top perturbed functions identified in IPA. The histogram is based on the top five enriched functions (depicted with the numbers 1–5) in female C57BL/6 mice after intratracheal exposure to CNT_{Small} or CNT_{Large}. The functions: cancer, cellular growth and proliferation, and cell death and survival were ranked in the top 3 following exposure either MWCNT, but the cellular movement function was ranked 4th after exposure to CNT_{Large}, whereas it was ranked 5th for CNT_{Small} exposures. Also, inflammatory response ranked 5th after exposure to CNT_{Large}, but ranked 10th after exposure to CNT_{Small}. The 4th ranked function after CNT_{Small} exposure was hematological system, development and function. A closer analysis of this function revealed a strong association with annotation terms related to the inflammatory response.

Table 2
Top 6 canonical pathways and networks in IPA affected by CNT_{Small} or CNT_{Large}.

Dose group	CNT_{Small}				CNT_{Large}			
	Canonical pathways		Networks		Canonical pathways		Networks	
	Name	# genes	Name	# genes	Name	# genes	Name	# genes
Day 1, 162 μg	LXR/RXR activation	26	Carbohydrate metabolism, lipid metabolism, small molecule biochemistry	32	Atherosclerosis signaling	26	Cell death and survival, cancer, hematological disease	30
	Atherosclerosis signaling	24	Organ morphology, lymphoid tissue structure and development	31	Acute phase response signaling	32	Gene expression	29
	Oxidative ethanol degradation III	7	Cell morphology, organismal development	31	LXR/RXR activation	25	Cell-to-cell signaling and interaction, tissue development, cardiac enlargement	27
	Hepatic fibrosis/hepatic stellate cell activation	27	Small molecule biochemistry, cellular assembly and organization, DNA replication recombination and repair	29	B cell development	10	Cellular movement, immune cell trafficking, cell signaling	27
	Pyrimidine ribonucleotides interconversion	8	Respiratory disease, RNA post-transcriptional modification	29	Calcium-induced T lymphocyte apoptosis	14	Post-translational modification, drug metabolism, lipid metabolism	27
	Acute phase response signaling	31	Cancer, hematological disease	29	Retinol biosynthesis	12	Cancer, inflammatory disease	26
Day 3, 162 μg	Aryl hydrocarbon receptor signaling	62	RNA post-transcriptional modification, connective tissue disorders	35	Hepatic fibrosis/hepatic stellate cell activation	59	Cellular function and maintenance, cardiac dilation	35
	Antigen presentation pathway	20	Cellular development, tissue development	35	IL-10 signaling	33	Cell cycle, cellular movement, cellular assembly and organization	35
	Hepatic fibrosis/hepatic stellate cell activation	61	Cell death and survival, organ development	34	Acute phase response signaling	65	Cellular assembly and organization, cell cycle, DNA replication recombination and repair	35
	Dendritic cell maturation	66	Carbohydrate metabolism, small molecule biochemistry, cellular movement	34	Dendritic cell maturation	60	Cellular movement, hematological system development and function, immune cell trafficking	34
	Crosstalk between dendritic cells and natural killer cells	36	Nucleic acid metabolism, small molecule biochemistry, amino acid metabolism	34	Pyrimidine deoxyribonucleotides de novo biosynthesis I	11	Cell morphology, cellular compromise, cellular growth and proliferation	34
	LXR/RXR activation	49	Cellular assembly and organization, DNA replication recombination and repair, cell cycle	34	Hypoxia signaling in the cardiovascular system	30	Cellular movement	34
Day 28, 162 μg	Hematopoiesis from pluripotent stem cells	4	Humoral immune response, protein synthesis, inflammatory response	23	IL-8 signaling	13	Molecular transport, developmental disorder	25
	Primary immunodeficiency signaling	4	Amino acid metabolism, molecular transport, small molecule biochemistry	14	Atherosclerosis signaling	9	Cancer, cardiovascular system development and function	23
			Cellular movement, hematological system development and function, immune cell trafficking	10	Retinol biosynthesis	5	Developmental disorder	22
			Cellular development, cellular growth and proliferation, connective tissue development and function	10	Triacylglycerol degradation	4	Connective tissue disorder, developmental disorder	23
			Cell morphology, cellular assembly and organization, cellular development	9	Chondroitin sulfate degradation	3	Cardiovascular system development and function, cellular development, cellular growth and proliferation	20
					Dermatan Sulfate Degradation	3	Cancer	18

Pathways and networks were identified in IPA and ranked based on their Benjamini–Hochberg Multiple Testing Correction P-value.

information, a closer analysis of genes involved in cholesterol synthesis and homeostasis was conducted at all doses and time points for MWCNT exposed mice, which revealed the consistent up-regulation of several genes involved in the 3-hydroxy-3-methylglutaryl-Coenzyme A (HMG-CoA) reductase pathway for both CNT types at the early time point (Supplementary Table 4). Down-regulation was also observed in the expression of membrane transporters ATP-binding cassette, sub-family A, member 1 (*Abca1*) and in ATP-binding cassette, sub-family G, member 1 (*Abcg1*) at post-exposure day 3. Both of these genes are involved in lipid homeostasis through cholesterol efflux. A linkage to fibrosis was observed through the regulation of hepatic fibrosis/hepatic stellate cell activation at the early time points following exposure to CNT_{Small} and CNT_{Large}. Although recognized for their role in hepatic fibrosis, many of the differentially regulated genes in this pathway play important roles in pulmonary fibrosis as well.

Finally, only two canonical pathways were perturbed 28 days post-exposure to CNT_{Small}; the small number of differentially expressed genes in each pathway indicates low pathway specificity (Table 2). In contrast to CNT_{Small}, genes involved in six pathways were affected 28 days post-exposure to CNT_{Large}. Interestingly, persistent changes in the expression of genes involved in inflammatory and atherosclerosis pathways were observed, indicating possible long-term effects.

Network analysis

Network analysis in IPA was employed to identify key regulatory genes and molecules. The top five networks at the high dose, days 1 and 3 post-exposure to either MWCNT (Table 2) were merged and network connections were visually depicted (Supplementary Fig. 9). For CNT_{Small} exposure, the primary network on post-exposure day 1 consisted of the core nodes *Myc*, *Cdkn1a* and *Egfr*. These genes are all involved in regulation of cellular proliferation and cell cycle; *Egfr* is also

highly implicated in fibrosis. Besides the core nodes, a distinct group of down-regulated genes clustered together (Supplementary Fig. 9.A, red circle), which belong to the dynein family. On day 3, the core nodes *Tnf* and *Gpcr* were identified (Supplementary Fig. 9.B). The latter is representative of the G protein-coupled receptor proteins, generally involved in signal transduction from the extracellular space to the cytoplasm. *Tnf* is a multifunctional proinflammatory cytokine belonging to the tumor necrosis factor superfamily, involved in the regulation of a wide spectrum of biological processes. Besides *Tnf* and *Gpcr*, several other small nodes were identified, but no distinct patterns were observed. For CNT_{Large} exposure, network analysis of post-exposure day 1 gene expression data revealed core nodes centered around *Myc*, *Nfkb1a*, *Gpcr* and *Nfkb complex* (Supplementary Fig. 9.C). *Myc* and *Gpcr* are both involved in regulation of cellular proliferation, whereas the *Nfkb* genes are important in cytokine production and cell survival. The network at post-exposure day 3 showed core nodes for *Tnf*, *Myc*, *Tgfb1*, *Igf1r* and *Gsk3b* (Supplementary Fig. 9.D). As in the day 1 network, core node genes were generally grouped into two categories: regulation of cellular proliferation (*Myc*, *Tgfb1*, *Igf1r* and *Gsk3b*) and inflammation (*Tnf*). However, most of these genes are highly pleiotropic. *Tgfb1*, through the SMAD signaling cascade, is also strongly associated with fibrosis. The common gene nodes identified further highlights the general high degree of similarity seen in the gene expression responses after CNT_{Small} and CNT_{Large} exposure.

Fibrosis gene signature

Fibrosis is a well-established endpoint in MWCNT-induced toxicity (Aiso et al., 2010; Mercer et al., 2011; Muller et al., 2005; Porter et al., 2010; Snyder-Talkington et al., 2013). In the present study, fibrosis (hepatic fibrosis/hepatic stellate cell activation) was observed as the top pathway hit following exposure to both CNT_{Small} and CNT_{Large}. This pathway was highly perturbed on day 3, with ligand-mediated effects on nuclear transcription across the entire pathway (Supplementary Fig. 10). The cells and genes involved in this pathway are similar to those involved in parenchymal injury to lungs, thus the induction of this pathway shows that MWCNT exposure may initiate a fibrotic response. Fibrosis induction is a highly multifactorial process and fibrosis-associated genes were grouped under several GO biological processes, including cellular growth and proliferation, response to wounding or cellular function and maintenance. We identified several matrix metallopeptidases (*Mmp10*, *Mmp11*, *Mmp12*, *Mmp13*, *Mmp14*, *Mmp15*, *Mmp19*, *Mmp3*, *Mmp8*, *Mmp9*) and tissue inhibitor of metalloproteinase (*Timp1*, *Timp2*, *Timp3*, *Timp4*), important for fibrogenesis and tissue remodeling, that were differentially regulated after exposure to both MWCNTs, primarily on post-exposure day 3. Also at the same time point, several genes involved in TGFβ signaling, which has been linked with the development of fibrosis, were differentially regulated following exposure to both MWCNTs (*Areg*, *Tgfbr2*, *Tgfbr3*, *Smad1*, *Smad6*, *Smad9*). However, *Tgfb1* and *Tgfb3* were regulated only after CNT_{Large} exposure. On post-exposure day 28, expression of many of the fibrosis-related genes had returned to baseline levels. However, an upstream analysis of the differentially regulated genes at this time point revealed that many of the genes affected by CNT_{Large} exposure (56 genes) were regulated by TGFB1. In comparison, only 14 TGFB1 regulated genes were identified following CNT_{Small} exposure. This indicates activation of fibrotic processes 28 days after exposure, but with an effect that was most prominent following CNT_{Large} exposure. Also, by using a list of genes linked to fibrosis described by Snyder-Talkington et al. (2013) and a by conducting a literature search, we identified 14 fibrosis-associated genes uniquely expressed on post-exposure day 28 following high dose CNT_{Large} exposure; *Arg1* (6.98-fold), *Igf1* (5.02-fold), *Lgals3* (3.13-fold), *Mmp12* (6.69-fold), *Mmp13* (2.39-fold), *Pde3a* (−1.95-fold), *Ptgir* (3.33-fold), *Smurf2* (−1.45-fold), T*nfrsf1b* (1.77-fold), *Vegfa* (−1.66-fold), *Eng* (−1.61-fold), *Jun* (1.87-fold), *Smad6* (−2.17-fold) and *Spp1* (6.41-fold). This unique expression pattern could indicate a chronic response related to the physicochemical properties of CNT_{Large}. This was emphasized in the upstream analysis, which revealed that exposure to CNT_{Large}, but not CNT_{Small}, induced differential expression of genes associated with bleomycin exposure, which is a strong inducer of pulmonary fibrosis (Supplementary Fig. 11A). Similarly, exposure to CNT_{Large}, but not CNT_{Small}, resulted in differential expression of genes associated with exposure to chrysotile asbestos, also a known inducer of fibrosis (Supplementary Fig. 11B).

qRT-PCR analysis

Eight genes belonging to immune response, oxidative stress or fibrosis were selected for validation by qRT-PCR (*Saa3*, *Il1α*, *Il6*, *Cxcl2*, *Ccl2*, *Hmox1*, *Mmp9* and *Sod2*). Validation was conducted at all doses and time points. The qRT-PCR results correlated well with the microarray results (Supplementary Table 5). A strong significant linear regression was found between qRT-PCR and microarray data ($P < 0.0001$) (Supplementary Fig. 12).

Histological examination of lungs

On post-exposure day 1, MWCNTs were present in the alveolar ducts and alveoli, and single macrophages were observed in the lung tissue of mice exposed to a high dose of both types of MWCNT (Fig. 6). Additionally, in the group exposed to CNT_{Large} perivascular neutrophilic infiltration and slight desquamation of bronchiolar epithelium were observed. Congestion was seen in the controls and MWCNT exposed groups and it was attributed to insufficient exsanguination of the carcasses.

On day 28 in the vehicle controls, minimal perivascular mononuclear-neutrophilic infiltration, fibroblasts and fibrocytes surrounding blood vessels and desquamation of bronchiolar epithelium were observed. The high-dose CNT_{Small} group showed interstitial pneumonia, characterized by lymphoid cell infiltration of both interstitium and alveolar lumina, small granulomas connected to alveolar walls or granulomatous alveolitis, and alveolar septal thickening due to type II pneumocyte hypertrophy and hyperplasia. Inflammatory cells and both intracellular and extracellular MWCNTs were observed in the alveoli. In the group exposed to the high-dose CNT_{Large} advanced interstitial pneumonia was observed, characterized by granulomas or granulomatous alveolitis, fibrosis and alveolar septal lymphoid infiltration. Fibrosis was observed following exposure to both types of MWCNT, but it was more severe in the high-dose CNT_{Large} group compared to the high-dose CNT_{Small} group (Figs. 6.J–L).

DNA damage

DNA strand breaks were evaluated through the comet assay in lungs from mice intratracheally exposed to CNT_{Small} or CNT_{Large} for all doses and on all time points (Fig. 7). A clear difference between CNT_{Small} and CNT_{Large} exposure was observed, as instillation of CNT_{Small} mainly affected the level of DNA strand breaks at the middle and high dose on post-exposure day 3 ($P < 0.001$), whereas instillation of CNT_{Large} affected all doses at post-exposure day 1 only ($P < 0.01$). We note that a single sample in the 162 μg dose group sampled 3 days after exposure to CNT_{Small} contained high levels of DNA damage, possibly driving the statistically significant difference between this group and the control group. However, careful examination of the sample revealed no signs of the apoptotic cells that were observed in samples subjected to incorrect thawing (Jackson et al., 2013). Thus, the high level of DNA damage was considered biological variance.

Free radical production

Acellular free radical production was assessed using a 2′,7′-dichlorofluorescein diacetate (DCFH-DA) assay, which measures

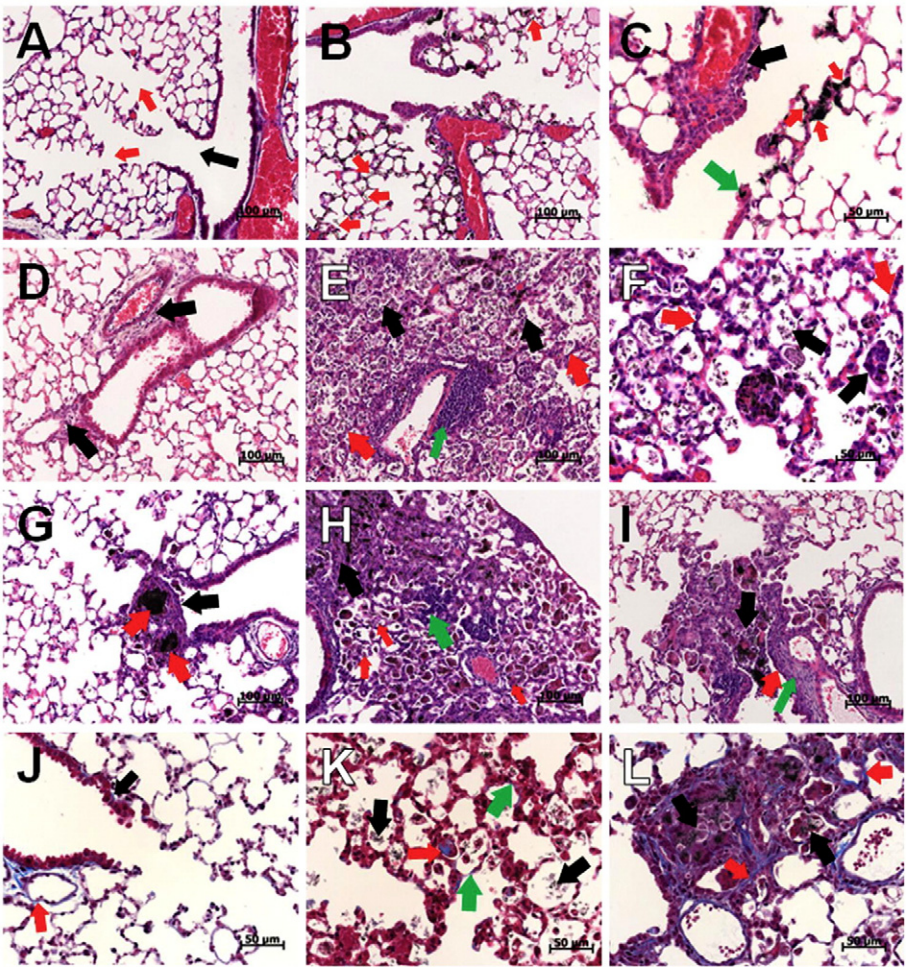

Fig. 6. Lung morphology. Representative HE or trichrome stained lung tissue sections from mice exposed to 0 or 162 μg/animal of CNT_{Small} or CNT_{Large}. (A)–(C) 1 day after instillation (a.i.) and (D)–(L) 28 days a.i. (A)–(I): HE staining; (J)–(L): trichrome staining. (A) Vehicle control: Normal structure, terminal bronchiole lumen (black arrow) bifurcates into two alveolar ducts (red arrows), congestion. Scale bar: 100 μm. (B) CNT_{Small} group: Extracellular CNT in centriacinar region (red arrows) and single macrophages. Scale bar: 100 μm. (C) CNT_{Large} group: MWCNTs in terminal bronchiole (green arrow) and in alveoli (red arrows), perivascular neutrophilic infiltration (black arrow) and slight desquamation of bronchiolar epithelium. Scale bar: 50 μm. (D) Vehicle control: Minimal perivascular mononuclear–neutrophilic infiltration (black arrows), and fibroblasts and fibrocytes surrounding blood vessels, desquamation of bronchiolar epithelium into the lumen of bronchiole. Scale bar: 100 μm. (E) CNT_{Small} group: Perivascular mononuclear cell infiltration (green arrow), interstitial pneumonia manifested as alveolar septal thickening due to type II pneumocyte hypertrophy and hyperplasia (red arrows), intra-alveolar lymphoid cell infiltration (black arrows), and aggregations of macrophages. Scale bar: 100 μm. (F) CNT_{Small} group: Interstitial and catarrhal pneumonia. Alveolar septal thickening (red arrows) due to fibroblasts and type II pneumocyte hypertrophy. Hyperplasia, intra-alveolar lymphoid cell infiltration and presence of the MWCNTs (black arrows); small granuloma in alveolar lumen. Scale bar: 50 μm. (G) CNT_{Large} group: Granuloma (black arrow) containing two aggregates of macrophages surrounding masses of the MWCNTs (red arrows) located at bifurcation of the terminal bronchiole into the two alveolar ducts. Scale bar: 100 μm. (H) CNT_{Large} group: Advanced interstitial and catarrhal pneumonia. Alveolar septal lymphoid cell infiltration (green arrow), alveolitis (red arrows) and prominent fibrosis (increase in observable connective tissue) (black arrow). Scale bar: 100 μm. (I) CNT_{Large} group: Interstitial pneumonia with fibrosis (green arrow), granuloma containing macrophages and neutrophils, and the MWCNTs located at bifurcation of the terminal bronchiole into the alveolar ducts (black arrow), attenuation of epithelium of terminal bronchiole (red arrow), desquamated bronchiolar epithelium in the lumen of bronchiole. Scale bar: 100 μm. (J) Vehicle control: small, normal amount of collagen in perivascular (red arrow) and peribronchial (black arrow) regions (blue color). Scale bar: 50 μm. (K) CNT_{Small} group: thickening of alveolar septa due to type II pneumocyte hypertrophy and hyperplasia, mild fibrosis within a small granuloma (red arrow) and in the alveolar septa (green arrows), and MWCNTs in alveolar lumen (black arrows). Scale bar: 50 μm. (L) CNT_{Large} group: interstitial pneumonia with alveolar septal fibrosis (red arrows), alveolitis, and intra-alveolar deposition of the MWCNTs (black arrows) Scale bar: 50 μm.

the DCFH oxidation from the MWCNT (Supplementary Fig. 13). Besides a slight increase in DCF observed at the highest concentration (135 μg/ml), CNT_{Large} did not induce free radical production. In contrast, a strong increase in DCF was observed even at the lowest concentration (1.4 μg/ml) for CNT_{Small}. A dose response was observed until dose 11.25 μg/ml, after which DCFH oxidation decreased with increasing dose. This decline is likely due to a quenching of the fluorescence by the MWCNT, as observed and described earlier for SWCNTs (Jacobsen et al., 2008).

Discussion

The physicochemical properties of MWCNTs, including the high aspect ratio, metal contamination, and straightness are considered important determinants of their toxicity. In this study, we investigated global changes in mRNA expression in lung tissue of female C57BL/6 mice 1, 3 or 28 days after intratracheal exposure to different doses of either CNT_{Small} or CNT_{Large}. Eight genes of interest were verified through qRT-PCR. Gene expression changes were interpreted in the context of other toxicological phenotypes that were measured in the same experimental setup, including inflammatory response, histological changes, DNA strand breaks and oxidative stress capacity. The physicochemical analyses of CNT_{Small} or CNT_{Large} revealed that the two MWCNTs differ in length, thickness, purity, surface area and level of agglomeration (Table 1). Despite these major differences in physical properties, the two MWCNTs induced remarkably similar changes in molecular phenotypes and gene expression, especially at post-exposure day 3. Both CNT_{Small} and CNT_{Large} exposure induced a strong increase in expression of genes involved in the inflammatory and acute phase response, which was sustained at post-exposure day 28 for both nanotube types. This

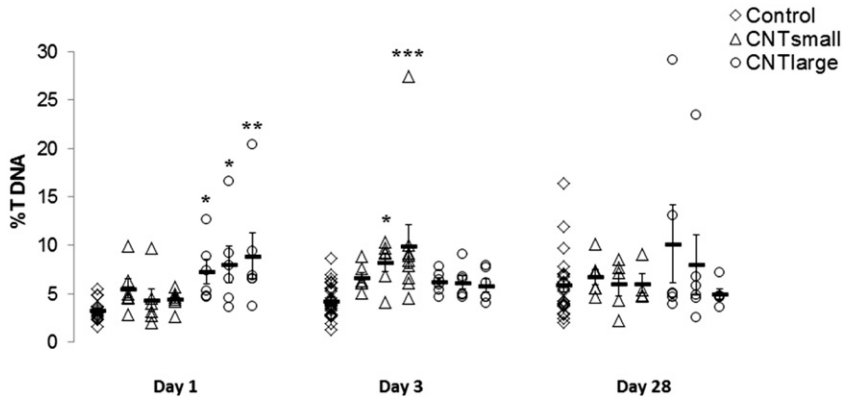

Fig. 7. %Tail DNA in C57BL/6 mouse lung following exposure to CNT_{Small} or CNT_{Large}. Each mouse in the dose group is represented. Under each time point, the dose groups are portrayed from left to right: 18 μg, 54 μg and 162 μg. Horizontal lines denote the means. *Statistically significantly different from vehicle instilled mice, $P < 0.05$. **Statistically significantly different from vehicle instilled mice, $P < 0.01$. ***Statistically significantly different from vehicle instilled mice, $P < 0.001$.

response is in concordance with the observed changes in BAL cell influx and lung morphology. Both CNT_{Small} and CNT_{Large} exposure resulted in the development of interstitial pneumonia on post-exposure day 28, however it was more sever with CNT_{Large}. The strong inflammatory and acute phase responses are not unique to MWCNT exposure. Similar responses have been observed following exposure to nano-titanium dioxide particles (nano-TiO_2) and nano-carbon black (nano-CB) particles via instillation or inhalation using experimental designs similar to that used in the present study (Bourdon et al., 2012a; Halappanavar et al., 2011; Husain et al., 2013; Jackson et al., 2011b). However, the number of differentially expressed genes was an order of magnitude greater following exposure to the two MWCNTs than following exposure to nano-TiO_2 and nano-CB, indicating stronger potency of MWCNT. The induction of an inflammatory response influenced several GO biological processes and IPA functions, e.g. 'cellular movement'. Many annotations under this category were associated with the movement of inflammatory cells, e.g. the annotations "cell movement of leukocytes" or "migration of phagocytes" and were perturbed by both MWCNTs; we speculate that small differences in the toxicological response could be masked by the strong inflammatory response. Other effects caused by CNT_{Small} and CNT_{Large} exposure included perturbation of lipid/cholesterol homeostasis, cell motility and cell cycle processes. However, notable differences were found that provide insight into differences in the potencies of these MWCNTs on pathological outcomes, namely a possible late-onset fibrotic response.

It has been documented that excessive collagen production and deposition of extra cellular matrix proteins during a persistent inflammatory response leading to lung injury (as reflected in BAL cell type composition, lung morphology and microarray analysis) may lead to development of fibrosis (Branton and Kopp, 1999; Strieter and Mehrad, 2009). Fibrosis has been an observed endpoint in several MWCNT studies (Aiso et al., 2010; Mercer et al., 2011; Muller et al., 2005; Porter et al., 2010; Ryman-Rasmussen et al., 2009; Wang et al., 2013). Snyder-Talkington et al. (2013) recently reported gene expression changes in male C57BL/6 mice exposed via pharyngeal aspiration to 10, 20, 40 or 80 μg of MWCNT Mitsui-7 and sampled 1, 7, 28 or 56 days post-exposure. Snyder-Talkington et al. found that Mitsui-7 exposure was related functionally to either fibrosis or inflammation and produced 2 gene lists based on this. A direct comparison of the 69 genes found to be related to fibrosis by Snyder-Talkington et al. with differentially expressed genes following exposure to either CNT_{Small} or CNT_{Large} in the present study revealed a high level of concordance, both to the results of Snyder-Talkington et al., but also between CNT_{Small} or CNT_{Large} exposed groups. However, it was found almost exclusively at the early time points (days 1 and 3) (Supplementary Table 6). A similar pattern emerged from our IPA analysis. Genes associated with the function 'cellular growth and proliferation' were perturbed 3 days after exposure to CNT_{Small} and CNT_{Large} (Fig. 5) with annotations such as "proliferation of fibroblast cell lines" and "proliferation of connective tissue". Although none of these effects were observed on post-exposure day 28, we observed subtle but important differences on day 28 following exposure to CNT_{Large}. A total of 10 genes from the list of genes from Snyder-Talkington et al. were differentially expressed at the high dose: *Arg1* (6.98-fold), *Igf1* (5.02-fold), *Lgals3* (3.13-fold), *Mmp12* (6.69-fold), *Mmp13* (2.39-fold), *Pde3a* (−1.95-fold), *Ptgir* (3.33-fold), *Smurf2* (−1.45-fold), T*nfrsf1b* (1.77-fold) and *Vegfa* (−1.66-fold) (Supplementary Table 6), whereas only one gene was differentially expressed following CNT_{Small} exposure: *Vegfa* (middle dose, −1.53-fold). A literature search for genes reported to be associated with fibrosis in general identified an additional 4 genes that were differentially expressed following CNT_{Large} exposure only on post-exposure day 28: *Eng* (−1.61-fold), *Jun* (1.87-fold), *Smad6* (−2.17-fold) and *Spp1* (6.41-fold). The connection between the 14 identified fibrosis-associated genes is depicted in a network analysis (Supplementary Fig. 14). The most differentially expressed gene among the 14 identified fibrosis-associated genes was *Spp1*, which codes for the osteopontin protein. Osteopontin has been suggested to be a marker for bleomycin-induced fibrosis in mice (Dave and Kaminski, 2005). It is an extracellular adhesion protein that is processed by extracellular proteases and has been associated with metastasis and mesothelioma carcinogenesis (Pass et al., 2005). Circulating osteopontin has also been shown to be predictive for the diagnosis of mesothelioma in humans (Pantazopoulos et al., 2013) and other asbestos-related diseases (Rodriguez Portal, 2012). It remains to be demonstrated whether osteopontin expression may be used to identify more harmful high aspect ratio nanomaterials.

The CNT_{Large}-induced late-onset of fibrosis was supported by the upstream analyses. TGFB1 was identified as the upstream regulator of several differentially expressed genes following CNT_{Large} exposure. This was to a lesser degree observed following CNT_{Small} exposure. Transforming growth factor β has been proposed as a key mediator in fibrosis through the SMAD signaling pathway (Sato et al., 2003; Flanders et al., 2002; Moeller et al., 2006). TGFB1 is involved in both fibroblast-to-myofibroblast conversion and epithelial–mesenchymal transition (EMT), both resulting in increased levels of myofibroblasts and subsequently increased collagen deposition (Wang et al., 2014; Willis and Borok, 2007; Willis et al., 2005; Kasai et al., 2005; Leask and Abraham, 2004). Several studies with MWCNT discussed an association between TGF-β and fibrotic lesions in the lungs (Chen et al., 2014; Ronzani et al., 2012; Wang et al., 2013, 2011b). Additionally, the upstream analyses also associated CNT_{Large} exposure with both bleomycin and chrysotile asbestos exposure. Bleomycin is a standard model for studying fibrosis (Peng et al., 2013; Moeller et al., 2006, 2008), and therefore the convergence of genes affected by both CNT_{Large} and

bleomycin suggests common molecular events driving fibrosis. This was not observed for CNT_{Small}. This is in concordance with the histological analysis. Although fibrosis was observed following exposure to both MWCNTs, it was more severe with CNT_{Large}. This association is also supported by the observation that only CNT_{Large} exposure induced differential expression of genes that are also differentially expressed following chrysotile asbestos exposure. CNT_{Small} and CNT_{Large} differ in many physicochemical parameters, including length and straightness. Studies have shown that the structure is highly important for MWCNT toxicity. For example, after exposing male SH rats to long and short MWCNT of similar width by intratracheal instillation Wang et al. (2013) observed that the long, but not the short, MWCNT induced fibrosis, probably through activation of TGF-β/Smad2/collagen III signal transduction. Porter et al. (2010) and Mercer et al. (2011) observed persistent fibrosis up to 56 days post-exposure in male C57BL/6 J mice exposed via pharyngeal aspiration to the long, thick MWCNT Mitsui-7. Comparing these studies to the result of the present study, we hypothesize that up-regulation of fibrosis related gene expression observed following CNT_{Large} exposure only, could be due to the structural differences between CNT_{Large} and CNT_{Small}. However, it should be noted that some studies observe no differences in the fibrotic potential between CNTs of different lengths (Muller et al., 2005; Ravichandran et al., 2011).

Snyder-Talkington et al. (2013) included an additional long-term time point (56 days) not analyzed in the present study. An order of magnitude higher number of differentially regulated genes were observed at this time point compared to day 28. This indicates effects of MWCNT Mitsui-7 exposure apparent only at time points later than day 28. We did not assess changes after 28 days, but given the physicochemical similarities between Mitsui-7 and CNT_{Large}, it is likely that CNT_{Large} also causes effects beyond 28 days. This emphasizes the need for long term studies. Although there is a general focus on length-dependent fibrotic effects, other factors such as purity, surface modifications and entanglement of the CNTs may also affect the fibrotic potential. Measurements of collagen deposition at later post-exposure time points are needed in order to confirm the development of fibrosis.

Following exposure to CNT_{Small} and CNT_{Large}, we noticed a large number of gene expression changes for serine proteinase inhibitors (serpins) (Supplementary Table 7), a superfamily of proteins where several members first were characterized as acute phase plasma protease inhibitors (Dickson and Alper, 1974). Serpins are now known to have functions in a wide range of tissues including the lungs (Silverman et al., 2001; Stein and Carrell, 1995). The greatest fold change was observed in the expression of the *Serpina3* gene, encoding α-1-antichymotrypsin. In the lung, this protein is important for the regulation of proteases released by leukocytes during an inflammatory response (Horvath et al., 2005; Travis et al., 1978). Neutrophil influx was significantly elevated at all doses and time points after exposure to either sized MWCNT, and the large up-regulation in expression of *Serpina3*s emphasizes a possible protective role of the protein against damage to the respiratory tract caused by proteolytic enzymes after MWCNT exposure. The expression of two *Serpina1*s was also significantly increased after exposure CNT_{Large}, but not after exposure to CNT_{Small}. Deficiency of α-1-antitrypsin, encoded by *Serpina1*s, renders the organism vulnerable to breakdown by neutrophil elastases and the deficiency has been correlated to chronic obstructive pulmonary disease (COPD) (Chappell et al., 2006; Dahl et al., 2002; Kueppers et al., 1969). In addition, studies have shown a correlation between cigarette smoking and increased levels of α-1-antitrypsin in the lungs (Linja-Aho et al., 2013; Olsen et al., 1975). The observed differential expression of *Serpina1*s in the present study may indicate that CNT_{Large} exposure could be a risk factor for COPD in a similar fashion to cigarette smoke. Long-term studies, preferably inhalation studies, are needed in order to confirm or refute this hypothesis.

The expression profiles following exposure to CNT_{Small} and CNT_{Large} were highly similar at post-exposure day 1. We recently published a toxicogenomic analysis of effects of in vivo and in vitro exposures to the MWCNT Mitsui-7 (Poulsen et al., 2013). These results enable the comparison between CNT_{Small}, CNT_{Large} and Mitsui-7. The in vivo experimental design in Poulsen et al. (2013) was identical to the design in the present study, although only one time point, day 1, was investigated, but animal exposures, experimentation and analysis of DNA microarray results were all performed separately from the present study. When examining the general expression profiles across the 3 different MWCNTs at post-exposure day 1 (fold change ±1.5, FDR corrected $P < 0.05$), we noted more similar expression patterns for CNT_{Small} and CNT_{Large} exposures than for Mitsui-7 and CNT_{Large} exposures (Supplementary Fig. 15). This trend was consistent for enriched IPA functions (Supplementary Fig. 16). DNA microarrays are powerful tools for understanding the global transcriptome, but due to the high number of comparisons made, some false-positive findings may occur. With that in mind, we narrowed our analysis to genes with greater changes in expression (fold change ± 3.0, FDR corrected $P < 0.05$). Overall, there was a high degree of concordance among the expression profiles following exposure to these different MWCNTs, especially at medium and high doses (Fig. 8). Genes whose transcription was similarly affected primarily belonged to inflammation and acute phase responses, as expected at this early time point. However, no clear differences between the gene expression profiles were observed. This highlights the reproducibility of the study design and of the DNA microarray experiment and analysis.

Differences in the expression of genes involved in the IPA function 'free radical scavenging' were observed between CNT_{Large}, and CNT_{Small}. Specifically, exposure to CNT_{Large}, but not to CNT_{Small}, resulted in differential expression of genes belonging to this function as early as post-exposure day 1 (Supplementary Fig. 8). The identified annotations under this category were "production of reactive oxygen species", "metabolism of reactive oxygen species" and "synthesis of reactive oxygen species", indicating the rapid generation of ROS in the lungs. We have previously shown that nano-CB produces ROS in vitro, and induces DNA strand breaks in the comet analysis in vivo and in vitro (Jacobsen et al., 2007, 2008, 2011). The mutation spectrum of nano-CB-induced mutations is consistent with generation by ROS. Therefore, there was a strong indication that the increased levels of DNA strand breaks observed in the comet assay were due to increased ROS production in the lung. Increased DNA strand break levels were observed at post-exposure day 1 after exposure to CNT_{Large}, but not to CNT_{Small}, thereby mimicking the early onset seen in the regulation of the function 'free radical scavenging'. CNT_{Large} does not contain many metal impurities and does not produce acellular ROS in contrast to CNT_{Small} (Supplementary Fig. 13 and Table 1), and therefore its ROS generating potential is likely to arise from its high aspect ratio inducing a biological ROS response. Long MWCNTs have been proven difficult to phagocytize by the alveolar macrophages, however the size range of CNT_{Small} and CNT_{Large} is too short to induce frustrated phagocytosis (Donaldson et al., 2010). Instead the increased level of ROS could be caused by disruption of phagosomes and lysosomes by CNT_{Large} exposure. This could ultimately lead to cell damage and difficulty in clearing the MWCNT from the lungs.

Conclusion

Analysis of pulmonary response to intratracheal exposure to CNT_{Small} or CNT_{Large}, two MWCNTs with very different physicochemical properties, revealed remarkably similar effects on the transcriptome, especially in the key processes inflammation and acute phase response. The gene expression changes observed correlated with BAL fluid cell type composition changes and lung histology changes. Both MWCNTs induced a large number of gene expression changes at the early time points (1 and 3 days), but also a lower, sustained response that was still apparent 28 days post-exposure. However, notable differences were found between the two MWCNTs in the expression of several genes associated with fibrosis and induction of fibrosis on post-

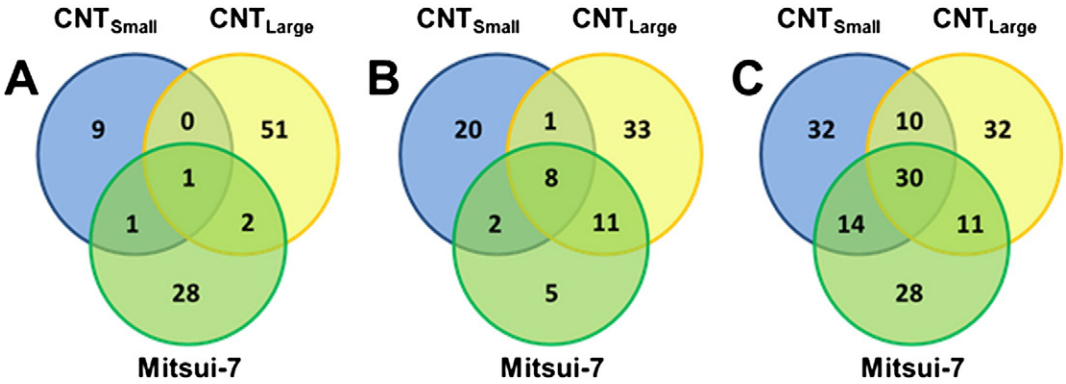

Fig. 8. Venn diagram of differentially expressed genes after exposure to CNT_{Small}, CNT_{Large} or Mitsui-7. $P < 0.05$ and fold change ± 3.0. Blue circle: CNT_{Small} exposure. Yellow circle: CNT_{Large} exposure. Green circle: Mitsui-7 exposure. (A) Dose 18 μg, day 1. (B) Dose 54 μg, day 1. (C) Dose 162 μg, day 1.

exposure day 28. Specifically, we identified a subset of 14 genes that were differentially regulated after exposure to CNT_{Large}, but not to CNT_{Small}, coinciding with a stronger fibrotic response to CNT_{Large} exposure. Thus, these genes could be candidates for biomarkers of fibrosis-related toxicity, and indicate a possible late-onset response that is specific to exposures to MWCNT with physicochemical compositions similar to CNT_{Large}.

Supplementary data to this article can be found online at http://dx.doi.org/10.1016/j.taap.2014.12.011.

Competing interests

The authors declare that they have no competing interests.

Funding

The project was supported by grants from the National Research Centre for the Working Environment in Denmark and the Danish NanoSafety Center, grant# 20110092173-3, the European Community's Seventh Framework Programme (FP7/2007-2013) under grant agreement #247989 (Nanosustain), and Health Canada's Chemical Management Plan-2 Nano research funds and Genomics Research and Development Initiative. The funders had no role in study design, data collection and analysis, decision to publish, or preparation of the manuscript.

Acknowledgments

The project was supported by grants from the National Research Centre for the Working Environment in Denmark grant # 20110092173-3 and the Danish NanoSafety Center, grant # 20110092173-3, the European Community's Seventh Framework Programme (FP7/2007-2013) under grant agreement #247989 (Nanosustain), and Health Canada's Chemical Management Plan-2 Nano research funds and Genomics Research and Development Initiative. The funders had no role in study design, data collection and analysis, decision to publish, or preparation of the manuscript. The authors thank M Guldbrandsen, L Petersen, and E Christiansen for technical assistance.

References

Aiso, S., Yamazaki, K., Umeda, Y., Asakura, M., Takaya, M., Toya, T., Koda, S., Nagano, K., Arito, H., Fukushima, S., 2010. Pulmonary toxicity of intratracheally instilled multi-wall carbon nanotubes in male Fischer 344 rats. Ind. Health 48, 783–795.

Beg, S., Rizwan, M., Sheikh, A.M., Hasnain, M.S., Anwer, K., Kohli, K., 2011. Advancement in carbon nanotubes: basics, biomedical applications and toxicity. J. Pharm. Pharmacol. 63, 141–163.

Benjamini, Y., Hochberg, Y., 1995. Controlling the false discovery rate: a practical and powerful approach to multiple testing. J. R. Stat. Soc. Ser. B Methodol. 57, 289–300.

Birch, M.E., Ku, B.K., Evans, D.E., Ruda-Eberenz, T.A., 2011. Exposure and emissions monitoring during carbon nanofiber production—part I: elemental carbon and iron-soot aerosols. Ann. Occup. Hyg. 55, 1016–1036.

Bourdon, J.A., Halappanavar, S., Saber, A.T., Jacobsen, N.R., Williams, A., Wallin, H., Vogel, U., Yauk, C.L., 2012a. Hepatic and pulmonary toxicogenomic profiles in mice intratracheally instilled with carbon black nanoparticles reveal pulmonary inflammation, acute phase response, and alterations in lipid homeostasis. Toxicol. Sci. 127, 474–484.

Bourdon, J.A., Saber, A.T., Jacobsen, N.R., Jensen, K.A., Madsen, A.M., Lamson, J.S., Wallin, H., Moller, P., Loft, S., Yauk, C.L., Vogel, U.B., 2012b. Carbon black nanoparticle instillation induces sustained inflammation and genotoxicity in mouse lung and liver. Part. Fibre Toxicol. 9, 5.

Branton, M.H., Kopp, J.B., 1999. TGF-beta and fibrosis. Microbes Infect. 1, 1349–1365.

Chappell, S., Daly, L., Morgan, K., Guetta, B.T., Roca, J., Rabinovich, R., Millar, A., Donnelly, S.C., Keatings, V., Macnee, W., Stolk, J., Hiemstra, P., Miniati, M., Monti, S., O'Connor, C.M., Kalsheker, N., 2006. Cryptic haplotypes of SERPINA1 confer susceptibility to chronic obstructive pulmonary disease. Hum. Mutat. 27, 103–109.

Chen, T., Nie, H., Gao, X., Yang, J., Pu, J., Chen, Z., Cui, X., Wang, Y., Wang, H., Jia, G., 2014. Epithelial-mesenchymal transition involved in pulmonary fibrosis induced by multi-walled carbon nanotubes via TGF-beta/Smad signaling pathway. Toxicol. Lett. 226, 150–162.

Cleveland, W., 1979. Robust locally weighted regression and smoothing scatterplots. J. Am. Stat. Assoc. 74, 829–836.

Cui, X., Hwang, J.T., Qiu, J., Blades, N.J., Churchill, G.A., 2005. Improved statistical tests for differential gene expression by shrinking variance components estimates. Biostatistics 6, 59–75.

Dahl, M., Tybjaerg-Hansen, A., Lange, P., Vestbo, J., Nordestgaard, B.G., 2002. Change in lung function and morbidity from chronic obstructive pulmonary disease in alpha1-antitrypsin MZ heterozygotes: a longitudinal study of the general population. Ann. Intern. Med. 136, 270–279.

Dahm, M.M., Evans, D.E., Schubauer-Berigan, M.K., Birch, M.E., Deddens, J.A., 2013. Occupational exposure assessment in carbon nanotube and nanofiber primary and secondary manufacturers: mobile direct-reading sampling. Ann. Occup. Hyg. 57, 328–344.

Dave, N.B., Kaminski, N., 2005. Analysis of microarray experiments for pulmonary fibrosis. Methods Mol. Med. 117, 333–358.

Dickson, I., Alper, C.A., 1974. Changes in serum proteinase inhibitor levels following bone surgery. Clin. Chim. Acta 54, 381–385.

Donaldson, K., Murphy, F.A., Duffin, R., Poland, C.A., 2010. Asbestos, carbon nanotubes and the pleural mesothelium: a review of the hypothesis regarding the role of long fibre retention in the parietal pleura, inflammation and mesothelioma. Part. Fibre Toxicol. 7, 5.

Driscoll, K.E., Costa, D.L., Hatch, G., Henderson, R., Oberdorster, G., Salem, H., Schlesinger, R.B., 2000. Intratracheal instillation as an exposure technique for the evaluation of respiratory tract toxicity: uses and limitations. Toxicol. Sci. 55, 24–35.

Erdely, A., Dahm, M., Chen, B.T., Zeidler-Erdely, P.C., Fernback, J.E., Birch, M.E., Evans, D.E., Kashon, M.L., Deddens, J.A., Hulderman, T., Bilgesu, S.A., Battelli, L., Schwegler-Berry, D., Leonard, H.D., McKinney, W., Frazer, D.G., Antonini, J.M., Porter, D.W., Castranova, V., Schubauer-Berigan, M.K., 2013. Carbon nanotube dosimetry: from workplace exposure assessment to inhalation toxicology. Part. Fibre Toxicol. 10, 53.

Flanders, K.C., Sullivan, C.D., Fujii, M., Sowers, A., Anzano, M.A., Arabshahi, A., Major, C., Deng, C., Russo, A., Mitchell, J.B., Roberts, A.B., 2002. Mice lacking Smad3 are protected against cutaneous injury induced by ionizing radiation. Am. J. Pathol. 160, 1057–1068.

Grosse, Y., Loomis, D., Guyton, K.Z., Lauby-Secretan, B., Ghissassi, F.E., Bouvard, V., Benbrahim-Tallaa, L., Guha, N., Scoccianti, C., Mattock, H., Straif, K., 2014. Carcinogenicity of fluoro-edenite, silicon carbide fibres and whiskers, and carbon nanotubes. Lancet Oncol. 15, 1427–1428.

Halappanavar, S., Jackson, P., Williams, A., Jensen, K.A., Hougaard, K.S., Vogel, U., Yauk, C.L., Wallin, H., 2011. Pulmonary response to surface-coated nanotitanium dioxide particles includes induction of acute phase response genes, inflammatory cascades, and changes in microRNAs: a toxicogenomic study. Environ. Mol. Mutagen. 52, 425–439.

Han, J.H., Lee, E.J., Lee, J.H., So, K.P., Lee, Y.H., Bae, G.N., Lee, S.B., Ji, J.H., Cho, M.H., Yu, I.J., 2008. Monitoring multiwalled carbon nanotube exposure in carbon nanotube research facility. Inhal. Toxicol. 20, 741–749.
Hedmer, M., Isaxon, C., Nilsson, P.T., Ludvigsson, L., Messing, M.E., Genberg, J., Skaug, V., Bohgard, M., Tinnerberg, H., Pagels, J.H., 2014. Exposure and emission measurements during production, purification, and functionalization of arc-discharge-produced multi-walled carbon nanotubes. Ann. Occup. Hyg. 58, 355–379.
Horvath, A.J., Irving, J.A., Rossjohn, J., Law, R.H., Bottomley, S.P., Quinsey, N.S., Pike, R.N., Coughlin, P.B., Whisstock, J.C., 2005. The murine orthologue of human antichymotrypsin: a structural paradigm for clade A3 serpins. J. Biol. Chem. 280, 43168–43178.
Huang, D.W., Sherman, B.T., Lempicki, R.A., 2009a. Systematic and integrative analysis of large gene lists using DAVID. Nucleic Acids Res. 37 (1), 1–13.
Huang, D.W., Sherman, B.T., Lempicki, R.A., 2009b. Systematic and integrative analysis of large gene lists using DAVID bioinformatics resources. Nat. Protoc. 4, 44–57.
Husain, M., Saber, A.T., Guo, C., Jacobsen, N.R., Jensen, K.A., Yauk, C.L., Williams, A., Vogel, U., Wallin, H., Halappanavar, S., 2013. Pulmonary instillation of low doses of titanium dioxide nanoparticles in mice leads to particle retention and gene expression changes in the absence of inflammation. Toxicol. Appl. Pharmacol. 269, 250–262.
Jackson, P., Hougaard, K.S., Boisen, A.M., Jacobsen, N.R., Jensen, K.A., Moller, P., Brunborg, G., Gutzkow, K.B., Andersen, O., Loft, S., Vogel, U., Wallin, H., 2011a. Pulmonary exposure to carbon black by inhalation or instillation in pregnant mice: effects on liver DNA strand breaks in dams and offspring. Nanotoxicology 6, 486–500.
Jackson, P., Hougaard, K.S., Vogel, U., Wu, D., Casavant, L., Williams, A., Wade, M., Yauk, C.L., Wallin, H., Halappanavar, S., 2011b. Exposure of pregnant mice to carbon black by intratracheal instillation: toxicogenomic effects in dams and offspring. Mutat. Res. 745, 73–83.
Jackson, P., Pedersen, L.M., Kyjovska, Z.O., Jacobsen, N.R., Saber, A.T., Hougaard, K.S., Vogel, U., Wallin, H., 2013. Validation of freezing tissues and cells for analysis of DNA strand break levels by comet assay. Mutagenesis 28, 699–707.
Jackson, P., Kling, K., Jensen, K.A., Clausen, P.A., Madsen, A.M., Wallin, H., Vogel, U., 2014. Characterization of genotoxic response to 15 multiwalled carbon nanotubes with variable physicochemical properties including surface functionalizations in the FE1-Muta(TM) mouse lung epithelial cell line. Environ. Mol. Mutagen. http://dx.doi.org/10.1002/em.21922 [Epub ahead of print].
Jacobsen, N.R., Saber, A.T., White, P., Moller, P., Pojana, G., Vogel, U., Loft, S., Gingerich, J., Soper, L., Douglas, G.R., Wallin, H., 2007. Increased mutant frequency by carbon black, but not quartz, in the lacZ and cII transgenes of muta mouse lung epithelial cells. Environ. Mol. Mutagen. 48, 451–461.
Jacobsen, N.R., Pojana, G., White, P., Moller, P., Cohn, C.A., Korsholm, K.S., Vogel, U., Marcomini, A., Loft, S., Wallin, H., 2008. Genotoxicity, cytotoxicity, and reactive oxygen species induced by single-walled carbon nanotubes and C(60) fullerenes in the FE1-Mutatrade markMouse lung epithelial cells. Environ. Mol. Mutagen. 49, 476–487.
Jacobsen, N.R., Moller, P., Jensen, K.A., Vogel, U., Ladefoged, O., Loft, S., Wallin, H., 2009. Lung inflammation and genotoxicity following pulmonary exposure to nanoparticles in ApoE−/− mice. Part. Fibre Toxicol. 6, 2.
Jacobsen, N.R., White, P.A., Gingerich, J., Moller, P., Saber, A.T., Douglas, G.R., Vogel, U., Wallin, H., 2011. Mutation spectrum in FE1-MUTA(TM) Mouse lung epithelial cells exposed to nanoparticulate carbon black. Environ. Mol. Mutagen. 52, 331–337.
Kasai, H., Allen, J.T., Mason, R.M., Kamimura, T., Zhang, Z., 2005. TGF-beta1 induces human alveolar epithelial to mesenchymal cell transition (EMT). Respir. Res. 6, 56.
Kerr, M.K., 2003. Design considerations for efficient and effective microarray studies. Biometrics 59, 822–828.
Kerr, M.K., Churchill, G.A., 2007. Statistical design and the analysis of gene expression microarray data. Genet. Res. 89, 509–514.
Klumpp, C., Kostarelos, K., Prato, M., Bianco, A., 2006. Functionalized carbon nanotubes as emerging nanovectors for the delivery of therapeutics. Biochim. Biophys. Acta 1758, 404–412.
Kobler, C., Saber, A.T., Jacobsen, N.R., Wallin, H., Vogel, U., Qvortrup, K., Molhave, K., 2014. FIB-SEM imaging of carbon nanotubes in mouse lung tissue. Anal. Bioanal. Chem. 406, 3863–3873.
Kueppers, F., Fallat, R., Larson, R.K., 1969. Obstructive lung disease and alpha-1-antitrypsin deficiency gene heterozygosity. Science 165, 899–901.
Leask, A., Abraham, D.J., 2004. TGF-beta signaling and the fibrotic response. FASEB J. 18, 816–827.
Lee, J.H., Lee, S.B., Bae, G.N., Jeon, K.S., Yoon, J.U., Ji, J.H., Sung, J.H., Lee, B.G., Lee, J.H., Yang, J.S., Kim, H.Y., Kang, C.S., Yu, I.J., 2010. Exposure assessment of carbon nanotube manufacturing workplaces. Inhal. Toxicol. 22, 369–381.
Lee, J.S., Choi, Y.C., Shin, J.H., Lee, J.H., Lee, Y., Park, S.Y., Baek, J.E., Park, J.D., Ahn, K., Yu, I.J., 2014. Health surveillance study of workers who manufacture multi-walled carbon nanotubes. Nanotoxicology 1–10.
Linja-Aho, A., Mazur, W., Toljamo, T., Nieminen, P., Ohlmeier, S., Ronty, M., Kinnula, V.L., 2013. Distribution and levels of alpha-1-antitrypsin in the lung and plasma in smokers and chronic obstructive pulmonary disease. APMIS 121, 11–21.
Livak, K.J., Schmittgen, T.D., 2001. Analysis of relative gene expression data using real-time quantitative PCR and the 2(−Delta Delta C(T)) Method. Methods 25, 402–408.
Ma-Hock, L., Treumann, S., Strauss, V., Brill, S., Luizi, F., Mertler, M., Wiench, K., Gamer, A.O., van, R.B., Landsiedel, R., 2009. Inhalation toxicity of multiwall carbon nanotubes in rats exposed for 3 months. Toxicol. Sci. 112, 468–481.
Mercer, R.R., Hubbs, A.F., Scabilloni, J.F., Wang, L., Battelli, L.A., Friend, S., Castranova, V., Porter, D.W., 2011. Pulmonary fibrotic response to aspiration of multi-walled carbon nanotubes. Part. Fibre Toxicol. 8, 21.
Methner, M., Hodson, L., Dames, A., Geraci, C., 2010. Nanoparticle Emission Assessment Technique (NEAT) for the identification and measurement of potential inhalation exposure to engineered nanomaterials—part B: results from 12 field studies. J. Occup. Environ. Hyg. 7, 163–176.
Methner, M., Beaucham, C., Crawford, C., Hodson, L., Geraci, C., 2012. Field application of the Nanoparticle Emission Assessment Technique (NEAT): task-based air monitoring during the processing of engineered nanomaterials (ENM) at four facilities. J. Occup. Environ. Hyg. 9, 543–555.
Moeller, A., Rodriguez-Lecompte, J.C., Wang, L., Gauldie, J., Kolb, M., 2006. Models of pulmonary fibrosis. Drug Discov. Today 3, 243–249.
Moeller, A., Ask, K., Warburton, D., Gauldie, J., Kolb, M., 2008. The bleomycin animal model: a useful tool to investigate treatment options for idiopathic pulmonary fibrosis? Int. J. Biochem. Cell Biol. 40, 362–382.
Muller, J., Huaux, F., Moreau, N., Misson, P., Heilier, J.F., Delos, M., Arras, M., Fonseca, A., Nagy, J.B., Lison, D., 2005. Respiratory toxicity of multi-wall carbon nanotubes. Toxicol. Appl. Pharmacol. 207, 221–231.
Murphy, F.A., Poland, C.A., Duffin, R., Al-Jamal, K.T., Ii-Boucetta, H., Nunes, A., Byrne, F., Prina-Mello, A., Volkov, Y., Li, S., Mather, S.J., Bianco, A., Prato, M., Macnee, W., Wallace, W.A., Kostarelos, K., Donaldson, K., 2011. Length-dependent retention of carbon nanotubes in the pleural space of mice initiates sustained inflammation and progressive fibrosis on the parietal pleura. Am. J. Pathol. 178, 2587–2600.
Olsen, G.N., Harris, J.O., Castle, J.R., Waldman, R.H., Karmgard, H.J., 1975. Alpha-1-antitrypsin content in the serum, alveolar macrophages, and alveolar lavage fluid of smoking and nonsmoking normal subjects. J. Clin. Invest. 55, 427–430.
Pantazopoulos, I., Xanthos, T., Boura, P., Syrigos, K., 2013. Mesothelin and osteopontin. Eur. Respir. J. 42, 557–558.
Park, E.J., Cho, W.S., Jeong, J., Yi, J., Choi, K., Park, K., 2009. Pro-inflammatory and potential allergic responses resulting from B cell activation in mice treated with multi-walled carbon nanotubes by intratracheal instillation. Toxicology 259, 113–121.
Pass, H.I., Lott, D., Lonardo, F., Harbut, M., Liu, Z., Tang, N., Carbone, M., Webb, C., Wali, A., 2005. Asbestos exposure, pleural mesothelioma, and serum osteopontin levels. N. Engl. J. Med. 353, 1564–1573.
Pauluhn, J., 2010a. Multi-walled carbon nanotubes (Baytubes): approach for derivation of occupational exposure limit. Regul. Toxicol. Pharmacol. 57, 78–89.
Pauluhn, J., 2010b. Subchronic 13-week inhalation exposure of rats to multiwalled carbon nanotubes: toxic effects are determined by density of agglomerate structures, not fibrillar structures. Toxicol. Sci. 113, 226–242.
Peng, R., Sridhar, S., Tyagi, G., Phillips, J.E., Garrido, R., Harris, P., Burns, L., Renteria, L., Woods, J., Chen, L., Allard, J., Ravindran, P., Bitter, H., Liang, Z., Hogaboam, C.M., Kitson, C., Budd, D.C., Fine, J.S., Bauer, C.M., Stevenson, C.S., 2013. Bleomycin induces molecular changes directly relevant to idiopathic pulmonary fibrosis: a model for "active" disease. PLoS One 8, e59348.
Poland, C.A., Duffin, R., Kinloch, I., Maynard, A., Wallace, W.A., Seaton, A., Stone, V., Brown, S., Macnee, W., Donaldson, K., 2008. Carbon nanotubes introduced into the abdominal cavity of mice show asbestos-like pathogenicity in a pilot study. Nat. Nanotechnol. 3, 423–428.
Porter, D.W., Hubbs, A.F., Mercer, R.R., Wu, N., Wolfarth, M.G., Sriram, K., Leonard, S., Battelli, L., Schwegler-Berry, D., Friend, S., Andrew, M., Chen, B.T., Tsuruoka, S., Endo, M., Castranova, V., 2010. Mouse pulmonary dose- and time course-responses induced by exposure to multi-walled carbon nanotubes. Toxicology 269, 136–147.
Poulsen, S.S., Jacobsen, N.R., Labib, S., Wu, D., Husain, M., Williams, A., Bogelund, J.P., Andersen, O., Kobler, C., Molhave, K., Kyjovska, Z.O., Saber, A.T., Wallin, H., Yauk, C.L., Vogel, U., Halappanavar, S., 2013. Transcriptomic analysis reveals novel mechanistic insight into murine biological responses to multi-walled carbon nanotubes in lungs and cultured lung epithelial cells. PLoS One 8, e80452.
Ravichandran, P., Baluchamy, S., Gopikrishnan, R., Biradar, S., Ramesh, V., Goornavar, V., Thomas, R., Wilson, B.L., Jeffers, R., Hall, J.C., Ramesh, G.T., 2011. Pulmonary biocompatibility assessment of inhaled single-wall and multiwall carbon nanotubes in BALB/c mice. J. Biol. Chem. 286, 29725–29733.
Reddy, A.R., Reddy, Y.N., Krishna, D.R., Himabindu, V., 2010. Pulmonary toxicity assessment of multiwalled carbon nanotubes in rats following intratracheal instillation. Environ. Toxicol. 27, 211–219.
Rittinghausen, S., Hackbarth, A., Creutzenberg, O., Ernst, H., Heinrich, U., Leonhardt, A., Schaudien, D., 2014. The carcinogenic effect of various multi-walled carbon nanotubes (MWCNTs) after intraperitoneal injection in rats. Part. Fibre Toxicol. 11, 59.
Rodriguez Portal, J.A., 2012. Asbestos-related disease: screening and diagnosis. Adv. Clin. Chem. 57, 163–185.
Ronzani, C., Spiegelhalter, C., Vonesch, J.L., Lebeau, L., Pons, F., 2012. Lung deposition and toxicological responses evoked by multi-walled carbon nanotubes dispersed in a synthetic lung surfactant in the mouse. Arch. Toxicol. 86, 137–149.
Ryman-Rasmussen, J.P., Tewksbury, E.W., Moss, O.R., Cesta, M.F., Wong, B.A., Bonner, J.C., 2009. Inhaled multiwalled carbon nanotubes potentiate airway fibrosis in murine allergic asthma. Am. J. Respir. Cell Mol. Biol. 40, 349–358.
Saber, A.T., Jacobsen, N.R., Mortensen, A., Szarek, J., Jackson, P., Madsen, A.M., Jensen, K.A., Koponen, I.K., Brunborg, G., Gutzkow, K.B., Vogel, U., Wallin, H., 2012. Nanotitanium dioxide toxicity in mouse lung is reduced in sanding dust from paint. Part. Fibre Toxicol. 9, 4.
Saber, A.T., Lamson, J.S., Jacobsen, N.R., Ravn-Haren, G., Hougaard, K.S., Nyendi, A.N., Wahlberg, P., Madsen, A.M., Jackson, P., Wallin, H., Vogel, U., 2013. Particle-induced pulmonary acute phase response correlates with neutrophil influx linking inhaled particles and cardiovascular risk. PLoS One 8, e69020.
Sato, M., Muragaki, Y., Saika, S., Roberts, A.B., Ooshima, A., 2003. Targeted disruption of TGF-beta1/Smad3 signaling protects against renal tubulointerstitial fibrosis induced by unilateral ureteral obstruction. J. Clin. Invest. 112, 1486–1494.
Shvedova, A.A., Kisin, E., Murray, A.R., Johnson, V.J., Gorelik, O., Arepalli, S., Hubbs, A.F., Mercer, R.R., Keohavong, P., Sussman, N., Jin, J., Yin, J., Stone, S., Chen, B.T., Deye, G., Maynard, A., Castranova, V., Baron, P.A., Kagan, V.E., 2008. Inhalation vs. aspiration of single-walled carbon nanotubes in C57BL/6 mice: inflammation, fibrosis, oxidative stress, and mutagenesis. Am. J. Physiol. Lung Cell. Mol. Physiol. 295, L552–L565.

Silverman, G.A., Bird, P.I., Carrell, R.W., Church, F.C., Coughlin, P.B., Gettins, P.G., Irving, J.A., Lomas, D.A., Luke, C.J., Moyer, R.W., Pemberton, P.A., Remold-O'Donnell, E., Salvesen, G.S., Travis, J., Whisstock, J.C., 2001. The serpins are an expanding superfamily of structurally similar but functionally diverse proteins. Evolution, mechanism of inhibition, novel functions, and a revised nomenclature. J. Biol. Chem. 276, 33293–33296.

Snyder-Talkington, B.N., Dymacek, J., Porter, D.W., Wolfarth, M.G., Mercer, R.R., Pacurari, M., Denvir, J., Castranova, V., Qian, Y., Guo, N.L., 2013. System-based identification of toxicity pathways associated with multi-walled carbon nanotube-induced pathological responses. Toxicol. Appl. Pharmacol. 272, 476–489.

Stein, P.E., Carrell, R.W., 1995. What do dysfunctional serpins tell us about molecular mobility and disease? Nat. Struct. Biol. 2, 96–113.

Strieter, R.M., Mehrad, B., 2009. New mechanisms of pulmonary fibrosis. Chest 136, 1364–1370.

The Nanogentox group, 2013. Nanogenotox (2013) Facilitating the Safety Evaluation of Manufactured Nanomaterials By Characterising Their Potential Genotoxicity Hazard.

Travis, J., Bowen, J., Baugh, R., 1978. Human alpha-1-antichymotrypsin: interaction with chymotrypsin-like proteinases. Biochemistry 17, 5651–5656.

Wang, X., Katwa, P., Podila, R., Chen, P., Ke, P.C., Rao, A.M., Walters, D.M., Wingard, C.J., Brown, J.M., 2011a. Multi-walled carbon nanotube instillation impairs pulmonary function in C57BL/6 mice. Part. Fibre Toxicol. 8, 24.

Wang, X., Xia, T., Ntim, S.A., Ji, Z., Lin, S., Meng, H., Chung, C.H., George, S., Zhang, H., Wang, M., Li, N., Yang, Y., Castranova, V., Mitra, S., Bonner, J.C., Nel, A.E., 2011b. Dispersal state of multiwalled carbon nanotubes elicits profibrogenic cellular responses that correlate with fibrogenesis biomarkers and fibrosis in the murine lung. ACS Nano 5, 9772–9787.

Wang, P., Nie, X., Wang, Y., Li, Y., Ge, C., Zhang, L., Wang, L., Bai, R., Chen, Z., Zhao, Y., Chen, C., 2013. Multiwall carbon nanotubes mediate macrophage activation and promote pulmonary fibrosis through TGF-beta/Smad signaling pathway. Small 9, 3799–3811.

Wang, P., Wang, Y., Nie, X., Braini, C., Bai, R., Chen, C., 2014. Multiwall carbon nanotubes directly promote fibroblast–myofibroblast and epithelial–mesenchymal transitions through the activation of the TGF-beta/Smad signaling pathway. Small. http://dx.doi.org/10.1002/smll.201303588 [Epub ahead of print].

Willis, B.C., Borok, Z., 2007. TGF-beta-induced EMT: mechanisms and implications for fibrotic lung disease. Am. J. Physiol. Lung Cell. Mol. Physiol. 293, L525–L534.

Willis, B.C., Liebler, J.M., Luby-Phelps, K., Nicholson, A.G., Crandall, E.D., du Bois, R.M., Borok, Z., 2005. Induction of epithelial–mesenchymal transition in alveolar epithelial cells by transforming growth factor-beta1: potential role in idiopathic pulmonary fibrosis. Am. J. Pathol. 166, 1321–1332.

Wu, H., Kerr, M.K., Cui, X., Churchill, G.A., 2003. MAANOVA: a software package for the analysis of spotted cDNA microarray experiments. In: Parmigiani, G. (Ed.), The Analysis of Gene Expression Data: Methods and Software. Springer, pp. 313–341.

Yamashita, K., Yoshioka, Y., Higashisaka, K., Morishita, Y., Yoshida, T., Fujimura, M., Kayamuro, H., Nabeshi, H., Yamashita, T., Nagano, K., Abe, Y., Kamada, H., Kawai, Y., Mayumi, T., Yoshikawa, T., Itoh, N., Tsunoda, S., Tsutsumi, Y., 2010. Carbon nanotubes elicit DNA damage and inflammatory response relative to their size and shape. Inflammation 33, 276–280.